sustainability

MDPI

Article

Impact of Various Operating Conditions on Simulated Emissions-Based Stop Penalty at Signalized Intersections

Suhaib Alshayeb *, Aleksandar Stevanovic and Nemanja Dobrota

Department of Civil & Environmental Engineering, Swanson School of Engineering, University of Pittsburgh, Benedum Hall, 3700 O'Hara Street, Pittsburgh, PA 15261, USA; stevanovic@pitt.edu (A.S.); ned47@pitt.edu (N.D.)
* Correspondence: sma115@pitt.edu

Abstract: Sustainability has become one of the most important goals when optimizing traffic signals. This goal is achieved through utilizing various objective functions to reduce sustainability metrics (e.g., fuel consumption and emissions). However, most available objective functions do not distinguish between the reduction mechanism of various types of emissions. Further, such functions do not consider the compound impact of multiple operational conditions (e.g., road gradient) influencing emissions on the optimized signal plans. This study derives a new Environmental Performance Index representing a surrogate measure for emission estimates that can be used as an objective function in signal timings optimization to reduce emissions under various operational conditions. The Environmental Performance Index is a linear combination of delays and stops. The key factor of the Environmental Performance Index is the emissions-based stop penalty, which represents an emission stop equivalency measured in seconds of delay. This study also uses traffic simulation and emission models to investigate the compound impact of several operational conditions on the stop penalty. Results show that the stop penalty varies significantly with all the investigated conditions and that the stop penalty is unique for different types of emissions. These findings may have significant implications on the current practice of sustainable signal timing optimization.

Keywords: emissions; signalized intersections; performance index; stop penalty; operating conditions; stops; sustainable signal control; signal timings optimization

Citation: Alshayeb, S.; Stevanovic, A.; Dobrota, N. Impact of Various Operating Conditions on Simulated Emissions-Based Stop Penalty at Signalized Intersections. *Sustainability* **2021**, *13*, 10037. https://doi.org/10.3390/su131810037

Academic Editor: Antonio Comi

Received: 31 July 2021
Accepted: 2 September 2021
Published: 8 September 2021

1. Introduction

Various emission types are determinantal to public health and the environment of the Earth as a whole. On the one hand, some pollutants (e.g., carbon monoxide) cause various health issues (e.g., severe respiratory and cardiovascular problems) [1,2], whereas on the other hand, other gases (e.g., carbon dioxide) cause damage to the environment (e.g., climate change) [3]. The industrial and population growth, coupled with rapid urbanization, has led to a drastic increase in automobiles and roadways. Consequently, fuel consumption from the transportation sector contributes to almost 55% of the total health-harmful emissions inventory in the U.S. and 28% of total U.S. greenhouse gas emissions [4,5].

Alleviating emissions burden through traffic signal control has been of interest because of its cost-effectiveness and non-reliance on encouraging motorists to adjust their driving habits (e.g., driving at lower speeds) [6,7]. Former studies [6,8] stated that extra emissions and fuel consumption at signalized intersections are intimately associated with unnecessary stop-events and extra seconds of delay while idling. However, the general practice of optimizing signals to minimize delay does not necessarily minimize extra stops; hence emissions could increase [6–8]. Thereby, several studies [9–11] have been conducted to find a Pareto-optimal signal timings solution to balance delay and stops. Over time, in some studies, the balancing between delay and stops has shifted gradually to a tradeoff process between delay and sustainable metrics (e.g., fuel consumption and emissions) [6,7,9–13].

However, most current literature does not differentiate between reducing fuel consumption and emissions [6,7,9–13]. Thus, a question that needs to be raised is whether minimizing fuel consumption truly minimizes a few, some, or all emission types? Results from earlier studies indicate that one or more emission types do not linearly correlate with fuel consumption [14,15]. Hence, we can infer that signal plans, which minimize fuel consumption, might reduce emissions but do not necessarily minimize various emission types.

The emergence of modern technologies to retrieve high-resolution (e.g., 10 Hz) signal performance measures (mobility and environmental) led to several objective functions being used to characterize vehicular emissions in the signal optimization process. Although introduced several decades ago, the Performance Index (*PI*), developed by Robertson in 1969 [16], is undoubtedly still one of the most widely used objective functions in the current signal timing optimization practice [17]. The *PI*, shown in Equation (1), is a linear combination of delays and stops with a *K*-factor that assigns a weight for each stop in seconds of delay.

$$PI = D + K \times S \quad (1)$$

where: *PI*—performance index (second), *D*—link delay (second), *K*—stop penalty (second), and *S*—number of stops on the link (second).

A few earlier studies on signal optimization [13,15,18] used the *PI* to find a balance between delay and fuel consumption because of their (somewhat) contradicting nature. Robertson et al. [18] confirmed that assigning more weight to each stop by increasing the *K* value reduces fuel consumption. Subsequent studies on the topic, summarized in [15], showed that the *K* value ranges from 26 to 228 s. Recent studies [19,20] showed that the *K*-factor is a function of various operating conditions that impact the fuel consumption estimates during a stop-event. The same recent studies also indicated that the *K* value derived for fuel consumption is not equal or linearly correlated with the *K* values derived for various vehicular emissions. Thus far, the *K*-factor has not been considered nor investigated from an emission point of view. This study attempts to fill this gap by achieving two primary objectives: 1—Deriving a universal environmental objective function using an emissions-based stop penalty as a tradeoff between vehicular delay and individual emission types, and 2—Investigating the impact of various vehicular, topological, operational, and external conditions on the proposed objective function. According to Banister's sustainable paradigm [21], the first objective of this study requires promoting the public acceptability of reasonable delay at signalized intersections instead of a minimum delay that is usually used as the main objective function to retime traffic signals. Consequently, this study contributes significantly to the research on sustainable signal timing optimization by introducing a family of implementable objective functions to minimize emissions. The derived objective function can be easily integrated into signal timing optimization practice to address environmentally driven signal retiming policies.

The structure of the study takes the form of seven sections, including this introductory section. The second part reviews the most notable studies concerning vehicular emissions and the optimization of traffic signals to minimize emissions and fuel consumption. Section three lays out the theoretical dimensions of the derived objective function. The methods used to investigate the impact of various conditions on the emissions-based stop penalty are provided in section four. The fifth section introduces and examines the findings of the research. Discussion of the findings is given in section six. Finally, the conclusions summarize the study, mention its limitations, and provide insights for future research.

2. Literature Review

Emission is a general term used to describe various gases and particles emitted into the air by multiple sources [22]. Such gases and particles can be detrimental solely or combined when two or more pollutants react to a harmful chemical compound. As mentioned previously, the transportation sector contributes significantly to harmful emissions. Hence, many studies have been conducted, on several aspects of transportation, to create a more sustainable transportation atmosphere. Some of these aspects are freight mobility [23,24],

bikes [25,26], and intelligent transportation systems [27–29]. Regarding the traffic signal control aspect, the past fifty years have seen increasingly accelerated progress in improving traffic signal timings to reduce emissions to help save people's lives and the habitability of our planet [6,7,9–15,30,31]. This section briefly reviews the literature from two critical aspects for this study: 1—Primary vehicular emission types, and 2—The most remarkable objective functions to decrease emissions and fuel consumption through signal timing optimization.

2.1. Major Vehicular Emissions

Vehicles do not always need to be moving to release emissions [32,33]; thus, vehicular emissions can be classified according to the vehicle operating mode in which emissions are emitted into three categories: 1—Evaporative "non-tailpipe" emissions are mainly driven by diurnal fuel evaporation, residual engine heat following vehicle operation inducing hot soak emissions, and running evaporative loss emissions that occur while vehicles are running [32]; 2—Refueling emission are volatile organic compound (VOC) vapor and entrained droplets displaced from the fuel tank ullage [33]; 3—Tailpipe "exhaust" emissions are the most evident because they are emitted while running the vehicle [34]. The focus of this study was on tailpipe emissions because they are profoundly emitted at road intersections constituting the most significant percentage of all types of vehicular emissions. Table 1 summarizes the primary tailpipe emissions and their impact on public health and the environment.

Table 1. Impact of primary vehicular emissions on public health and environment.

Emission Type	Emission Category	Effect
Carbon Monoxide (CO)	Tailpipe	Reduces the amount of oxygen transported in the bloodstream to critical organs such as the heart and brain [35]. It can also cause dizziness, confusion, unconsciousness, and death at high concentrations [35].
Carbon dioxide (CO_2)	Tailpipe	Increases the Earth's temperature (global warming), causing climate change [36]. We note here that CO_2 is not an air pollutant, but it is one of the major greenhouse emissions emitted by vehicles.
Nitrogen oxides (NO and NO_2, together called NOx)	Tailpipe	Contributes to global warming [3], acid rain [37], and depletion of the ozone layer [38]. It also damages the human respiratory tract and increases a person's vulnerability to respiratory infections and asthma [39].
Hydrocarbons (HC), also known as volatile organic compounds (VOCs) or non-methane hydrocarbons (NMHC) [23]	Evaporative, refueling, and tailpipe	Reacts with nitrogen oxides in the presence of sunlight to form ground-level ozone, which can trigger various health problems, including chest pain, coughing, throat irritation, and congestion [40].
Particulate matter of size < 10 microns (PM_{10}) and <2.5 microns ($PM_{2.5}$) including black carbon (BC)	Tailpipe	PM caused several health issues, including cardiovascular effects, such as cardiac arrhythmias and heart attacks, and respiratory effects, such as asthma attacks and bronchitis [2].

Despite the importance of particulate matter (PMs) as harmful pollutants, the PMs were not considered in this study because most commercially available emissions models do not provide PM estimates for vehicles powered by gasoline. Despite the primary source of PMs generation being diesel-powered vehicles [41], most available emissions models do not estimate high-resolution (second-by-second) PMs measures for such vehicles. Although a few models (e.g., VT-Micro [42]) can estimate second-by-second PMs measures for HDDVs, the publicly available versions of such models are not suitable to conduct the large number of scenarios performed in this study (discussed later).

One way to classify road intersections is based on the type of traffic control devices. That involves two types of intersections: 1—Unsignalized intersections, where the right of the way is defined using the traffic control signs (e.g., stop or yield), and 2—Signalized intersections, where traffic lights are used to spatially and temporally allocate conflicting traffic streams [43]. The design of both intersection types does not follow an exact rule. Still, it considers the effect of multiple factors (e.g., physical space and signal timings) simultaneously to provide safe and efficient mobility [43]. This study focuses on the excess tailpipe emissions induced by non-optimal signal timings at signalized intersections. Moreover, the proposed methodology applies to various signalized intersections' designs.

2.2. Relevant Objective Functions

A large and expanding body of literature has investigated reducing vehicular emissions through the retiming of traffic signals. This subsection summarizes the objective functions used in the most notable signal optimization studies endeavoring to reduce fuel consumption and emissions. The studies reviewed here have used a common approach in their models by integrating a traffic model, fuel consumption and emissions model, and an optimization method to improve an objective function. Table 2 summarizes the reviewed studies according to those integrated elements.

Table 2. Most notable objective functions used in signal timings optimization to reduce fuel consumption and emissions.

Study	Traffic Model	Emissions Model	Optimization Technique	Optimized Parameter(s)	Objective Function	Nomenclature
Li et al. [9]	Analytical	Analytical	Calculus-based	Delay, fuel consumption, and emissions	$PI = \alpha \frac{D}{Di} + \beta \frac{F}{Fi} + \gamma \frac{E}{Ei}$	D: delay, F: fuel consumption, E: emissions, α, β, and γ: relative significance weights, Di, Fi and Ei: values of D, F and E for the initial signal-timing scenario
Oda et al. [44]	AVENUE	Analytical	Calculus-based	Delay, stops, and CO_2	$PI = \sum(\alpha \cdot d + \beta \cdot S)$	D: delay, S: stops, α and β: weight coefficients
Stevanovic et al. [6]	VISSIM	CMEM	Genetic algorithm	Fuel consumption and CO_2	$FR(t) = \varnothing \cdot (K \cdot N \cdot V + \frac{P}{\mu}) \cdot \frac{1}{44}$ $CO_2 = a \cdot FR + r$	$FR(t)$: fuel rate, $\varnothing$: stoichiometric fuel/air equivalence ratio, K: the engine friction factor, N: engine speed, V: engine displacement, P: engine power output, μ: a measure of indicated efficiency, and 44—the lower heating value of typical gasoline. a and r are the CO_2 index coefficients
Park et al. [7]	CORSIM	VT-Micro	Genetic algorithm	Fuel consumption and emissions (as a posteriori)	$\ln(FC) = \left\{ \sum_{i=0}^{3} \sum_{j=0}^{3} L_{i,j}^{e} \cdot s^i \cdot a^j \right.$	$L_{i,j}^{e}$: represent model regression coefficients for fuel consumption (FC) at speed (s) exponent i and acceleration (a) exponent j
Ma and Nakamura [14]	Analytical	Analytical	Calculus-based	NOx	$NOx = \left(\frac{d_{NOx_i}}{d_t} \cdot \sum_{i=1}^{n} D_s \right) + (NOx_d + NOx_a)$	$\frac{d_{NOx_i}}{d_t}$: emission rate of idle mode for vehicle i, D_s: stopped delay, n: stops, d: deceleration phase, a: acceleration phase.
Kwak et al. [11]	TRANSIMS	VT-Micro	Genetic algorithm	Fuel consumption	$\ln(FC) = \left\{ \sum_{i=0}^{3} \sum_{j=0}^{3} L_{i,j}^{e} \cdot s^i \cdot a^j \right.$	Same as Park et al. [7]
Zhang et al. [45]	Cell Transmissions model (CTM)	Analytical	Genetic algorithm	Emissions as bulk	$E_{j,k_f} = \sum_{i=1}^{I} \left\{ \frac{t_{i,j,k_f}}{T_{j,k_f}} \cdot ER_i \right\}$	E_{j,k_f}: average emission rate on link j for speed range k on facility f, ER_i: VSP modal average emission rate for VSP Mode i, VSP: vehicle specific power, t: time spent in VSP mode, T: total travel time on link
Lv et al. [46]	Analytical	MOVES and Analytical	Genetic algorithm	CO	$CO = \begin{cases} 1791.49 \cdot D^{0.04153}, & v = 45 \\ 1331.28 \cdot D^{0.03099}, & v = 40 \\ 883.5 \cdot D^{0.02133}, & v = 35 \end{cases}$	D: delay, v: speed
Khalighi and Christofa [47]	Analytical and AIMUSN	Analytical	Mixed-integer nonlinear program	Emissions as bulk	$E_{j,k_f} = \sum_{i=1}^{I} \left\{ \frac{t_{i,j,k_f}}{T_{j,k_f}} \cdot ER_i \right\}$	Same as Zhang et al. [38]
Osorio and Nanduri [48]	Analytical and AIMUSN	Analytical	Metamodel simulation-based	Travel time and emissions (as bulk)	$f = f^t \frac{w^t}{n^t} + f^{CO2} \frac{w^{CO2}}{n^{CO2}} + f^{NOx} \frac{w^{NOx}}{n^{NOx}} + f^{VOC} \frac{w^{VOC}}{n^{VOC}} + f^{PM} \frac{w^{PM}}{n^{PM}}$	f^T, f^{CO2}, f^{NOx}, f^{VOC}, f^{PM}: expected travel time and various emission types, w^T, w^{CO2}, w^{NOx}, w^{VOC}, w^{PM}: economic weighting parameters, n^T, n^{CO2}, n^{NOx}, n^{VOC}, n^{PM}: normalization constants for travel time and emission types
Han et al. [49]	Lighthill-Whitham-Richards (LWR) model	Analytical	Mixed-integer linear program	Throughputs and emissions (as a posteriori)	$f = \max \sum_{k=1}^{m} \frac{1}{k+1} \sum_{l_i \in \tau} q_i^k$	M: total number of time intervals, τ: prescribed set of links, q_i: the flow at which vehicles exit link Ii

There are two types of traffic models used in the reviewed studies, which are deterministic (also known as analytical or macroscopic) models (e.g., [50,51]) and stochastic (also known as microscopic) simulation models of more realistic real-world traffic through the application of computer programs (e.g., [52]). Similarly, analytical (with pre-computed fuel consumption and emissions factors) (e.g., [53]) and microscopic (second-by-second) (e.g., [54]) fuel consumption and emissions models were utilized to estimate the objective function and measure the improvement in emission savings. Although utilizing macroscopic models is computationally efficient, approaches of this kind carry various well-known limitations, such as the inability to capture the individual characteristics of drivers; hence, they generate less accurate emissions estimates. Therefore, studies that used high-resolution models seem to be more reliable than those that utilized analytical models. The optimization methods used by research presented here can be broadly classified into three techniques: 1—Calculus-based using the first derivative, 2—Guided random search utilizing the Genetic Algorithm (GA) approach, and 3—The enumerative technique as a common way to solve mixed-integer mathematical programs.

Several objective functions were developed and optimized using one of the optimization techniques mentioned above. Those objective functions represent either fuel consumption and emissions directly (e.g., [6,7]), performance indexes (PIs) associated directly with fuel consumption emissions (e.g., [9,44]), or a combination of both (e.g., [48]). A major criticism of using fuel consumption and emissions directly as an objective function is that it fails to recognize the difficulties that arise when attempting to estimate fuel consumption and emissions in a specific site in the field. Another problem with this approach is that it might reduce emissions at the expense of worsening mobility metrics (e.g., delay). The former issue also applies to the objective functions where direct mobility and emissions measures are combined. Moreover, regardless of their objective function, most of the literature lacks accuracy because they do not consider various operational conditions (e.g., vehicle type and road gradient) that impact the emissions estimates at signalized intersections. Therefore, this study derived an environmental objective function that can be tailored to a specific emission type and considers various operational conditions.

The critical element of the derived objective function is the emissions-based stop penalty. Furthermore, the study investigates the combined impact of various operational conditions: vehicle type, the proportion of heavy vehicles in the fleet, driving behavior, road gradient, cruising speed, and wind effect on the emissions-based stop penalty. The investigation was done using a full-factorial experimental design representing different operational conditions. The traffic simulation Vissim [52] was employed to perform the dynamics part of the experiments and generate vehicles' trajectories (also known as floating car data) for numerous scenarios. Those trajectories were then used to estimate emissions (HC, CO, NOx, and CO_2) from the Comprehensive Modal Emission Model (CMEM) [54]. Finally, the emissions-based stop penalty was computed for each tested emission type under all investigated scenarios.

3. Environmental Objective Function

This section presents the derivation of the proposed objective function. For the reader's convenience, Table 3 summarizes the notation used in this section.

The original definition of the *K*-factor referred to the number of seconds of delay that is equivalent to a single stopping maneuver [16]. A few studies [15,19,20] redefined the *K*-factor as the number of seconds of idling delay (referred to as stopped delay hereafter) that consume the same amount of fuel consumed during a stop. This research defines the stop penalty as the number of seconds of stopped delay equivalent to excess emissions caused by the action of stopping (deceleration and acceleration phases, referred to as a stop hereafter), and we call this stop penalty K_E. Consequently, the K_E value required to reduce a specific emission type was derived based on the amount of a specific gas emitted during the three driving modes of a complete stop. These modes are deceleration, idling, and acceleration, and they all form what is known as the vehicular stop profile shown

in Figure 1. The total amount of a particular gas emitted during a stop is expressed in Equation (2), where all units are identical and can be expressed in gallons, liters, or grams:

$$E_i = E_{D_i} + E_{I_i} + E_{A_i} \quad (2)$$

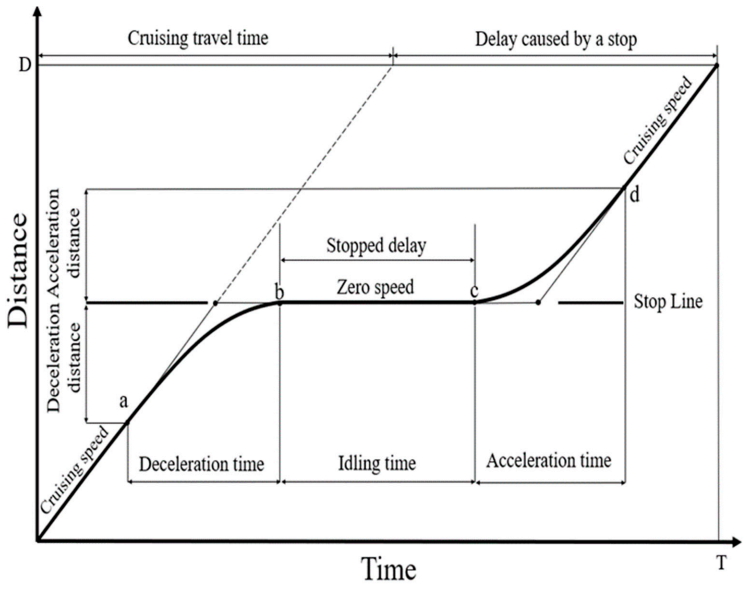

Figure 1. Time-distance (stop) profile of a full stop.

Table 3. Nomenclature.

Variable	Description
E_i	Total amount of emission type i emitted during an entire stop (gallons, liters, or grams)
E_{D_i}	Total amount of emission type i emitted during deceleration mode (gallons, liters, or grams)
E_{I_i}	Total amount of emission type i emitted during idling mode (gallons, liters, or grams)
E_{A_i}	Total amount of emission type i emitted during acceleration mode (gallons, liters, or grams)
i	Emission type
K_{Ee}	Ratio between the amount of emission induced by stop and one caused by stopped delay
E_{DA}	Emissions during deceleration and acceleration modes (gallons, liters, or grams)
K_E	Emissions-based stop penalty (seconds)
T_I	Idling phase duration (seconds)
t_1 and t_2	Any two-time points where: $t_1 < t_2$ (seconds)
E	General term for emission despite of the emission type (gallons, liters, or grams)
E_r	Emission rate (gallons, liters, or grams per unit time)
t	Any point of time (seconds)
Δ_t	Time interval between any two-time points (seconds)
$a, b, c, and\ d$	Time points of starts and ends of various driving phases, as characterized in Figure 1 (seconds)
$Env - PI$	Environmental Performance Index (seconds)
j	Link
n	Total number of links
$CO - PI$	Carbon monoxide Performance Index (seconds)
D_j	Stopped delay on link j (seconds)
S_j	Total stops on link j (seconds)
e_i	Amount of emission type i estimated by CMEM (grams)
a_i and r_i	Index coefficients of emission type i
FR	Fuel rate (grams/sec)
$\emptyset(t)$	Stoichiometric fuel/air equivalence ratio
$K(t)$	Engine friction factor
$N(t)$	Engine speed (revolutions/seconds)
V	Engine displacement (liters)
$P(t)$	Engine power output (kW)
μ	Indicated efficiency (default value is 0.4)

To compute how many seconds of delay emit the same amount of a particular emission type caused by a stop, we need to find the ratio (K_{Ee}) between the amount of that emission type induced by the stop and the one caused by the stopped delay (Figure 1). Thus, it is essential to separately identify extra emissions caused by the stop, represented as E_{DA} (E_D + E_A), from those emitted during the stopped delay, represented as E_I. As all ratios, the K_{Ee} expressed in Equation (3) is unitless. Hence, when the E_I is divided by the idling phase duration (T_I), which varies based on the duration of the red interval, the result gives the number of seconds of stopped delay that emit the same excess emissions equivalent to a stopping event. That is what we define as the emissions-based stop penalty (K_E) (given in Equation (4)).

$$K_{Ee} = \frac{E_{DA}}{E_I} \tag{3}$$

$$K_E = \frac{E_{DA}}{\frac{E_I}{T_I}} = \frac{E_{DA} \cdot T_I}{E_I} \tag{4}$$

Figure 2 shows instantaneous (second-by-second) emitting rates of four emission criteria (HC, CO, NOx, and CO_2) during a complete simulated stop from 20 mph and back. We note here that Figure 2 is from a single simulated trajectory in Vissim, where emission estimates were estimated by using the CMEM software for the same simulated trajectory. Area 1, Area 2, and Area 3 represent the emissions during the deceleration, idling, and acceleration phases, respectively. The sum of those three areas under each emission criterion's curve is the total amount of that criterion emitted during a stop for a particular vehicle under specific operational conditions (e.g., cruising speed, road gradient). Areas 1–3 under any curve can be found by doing a definite integral of the time-dependent variable emission rate (E_r) curve between any two-time points t_1 and t_2:

$$E = \int_{t1}^{t2} E_r(t).dt \tag{5}$$

With the availability of second-by-second emission estimates, the amount of emissions caused by a stop (Equation (3)) can be computed as the sum of the emissions in every time interval (Δt) of driving (Equation (6)), where points a, b, c, and d are the starts and ends of various driving phases as characterized in Figure 1.

$$E_i = \sum_{t=a}^{b} E_{D_i}(t) \cdot \Delta t \; + \sum_{t=b}^{c} E_{I_i}(t) \cdot \Delta t + \sum_{t=c}^{d} E_{A_i}(t) \cdot \Delta t \tag{6}$$

The K_E can then be calculated by substituting the values of E_{DA} and E_I with their values from Equation (6), as follows:

$$K_E = \frac{(\sum_{t=a}^{b} E_{D_i}(t) \cdot \Delta t \; + \; \sum_{t=c}^{d} E_{A_i}(t) \cdot \Delta t) \cdot \; \sum_{i=b}^{c} \Delta t}{\sum_{t=b}^{c} E_{I_i}(t) \cdot \Delta t} \tag{7}$$

It is apparent from Equation (7) that the K_E varies based on the amount of emission during each of the deceleration, idling, and acceleration modes. Furthermore, Figure 2 shows that various emission criteria are emitted at different rates during each driving mode. Thus, it is anticipated that K_E would vary for different emission types. For that reason, we define an Environmental Performance Index (Env-PI) as a generic objective function that can be derived to reduce a particular emission criterion (E) (e.g., HC, CO, NOx, and CO_2) caused by stopping at traffic signals. The Env-PI for a network can be computed by summing the Env-PIs for all movements in the network as follows:

$$Env - PI = \sum_{j=1}^{n} D_j + \frac{(\sum_{t=a}^{b} E_{D_i}(t) \cdot \Delta t \; + \; \sum_{t=c}^{d} E_{A_i}(t) \cdot \Delta t)_j}{(\frac{\sum_{t=b}^{c} E_{I_i}(t) \cdot \Delta t}{\sum_{t=b}^{c} \Delta t})_j} \cdot S_j \tag{8}$$

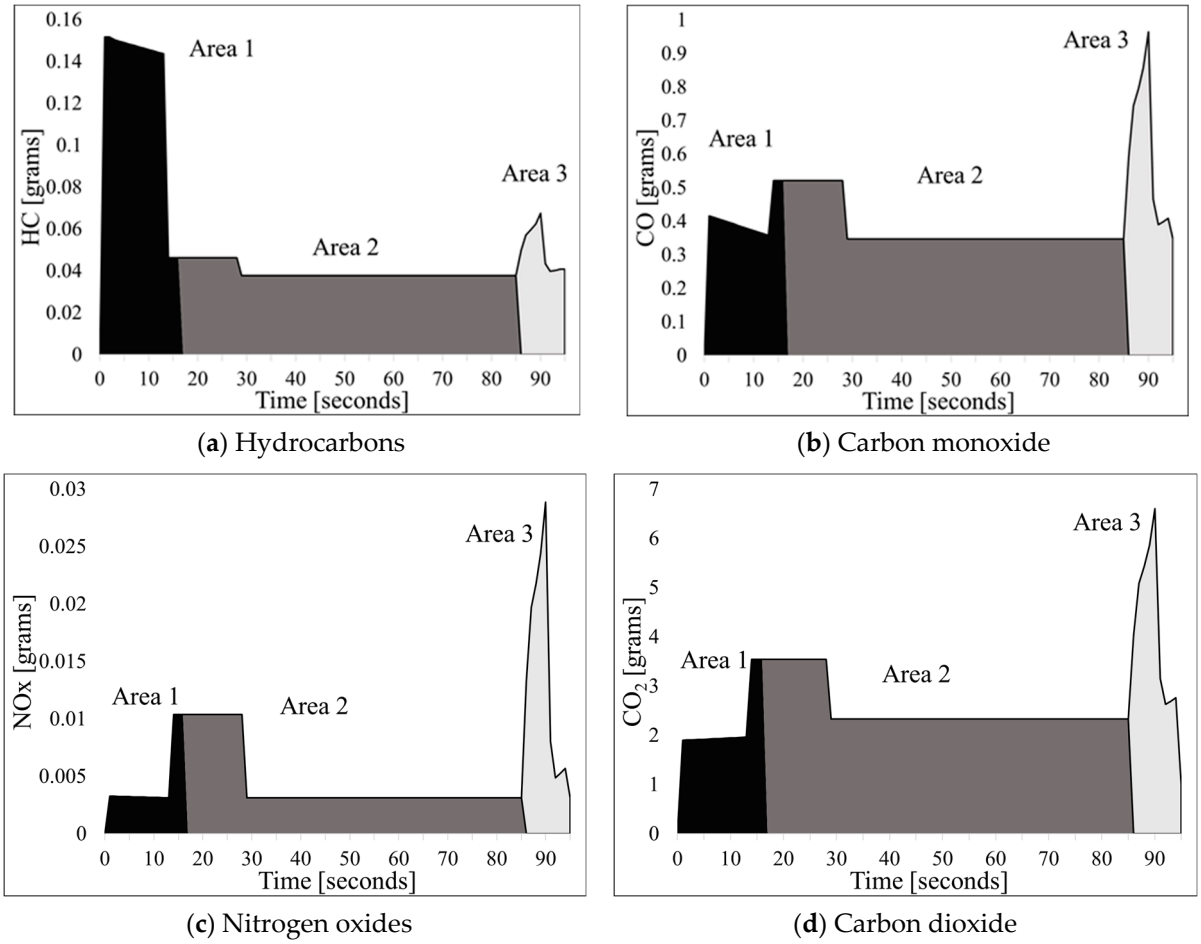

Figure 2. Various emission type footprints caused by a single stop (20-mph—zero—20-mph).

Consequently, the Env-PI for a particular emission type can be defined as one of a family of similar Env-PIs. For example, HC-PI, CO-PI, NOx-PI, and CO_2-PI are all members of the Env-PI family that are explicitly derived to reduce HC, CO, NOx, and CO_2, respectively. For the sake of giving an example that Env-PI could be derived for any emission criterion, Equation (9) shows a CO-PI. That suggests that the CO-PI may result in different signal timings for a particular network than those derived for any other Env-PIs. Therefore, the relevant Env-PI should be used when optimizing signals to reduce a specific emission criterion.

$$CO - PI = \sum_{j=1}^{n} D_j + \frac{\left(\sum_{t=a}^{b} CO_{D_i}(t)\cdot\Delta t \; + \; \sum_{t=c}^{d} CO_{A_i}(t)\cdot\Delta t\right)_j}{\left(\frac{\sum_{t=b}^{c} E_{I_i}(t)\cdot\Delta t}{\sum_{t=b}^{c}\Delta t}\right)_j}\cdot S_j \tag{9}$$

Our current study uses the microscopic power demand emissions model CMEM to estimate second-by-second emissions [54]. CMEM estimates various emissions as a function of the fuel rate, which depends on the air-fuel ratios occurring during internal fuel combustion. Equation (10) shows the general form of the equation used to estimate a particulate emission criterion E_i [54].

$$e_i = a_i \cdot FR + \; r_i \tag{10}$$

$$FR(t) = \varnothing(t)\cdot\left(K(t)\cdot N(t)\cdot V + \frac{P(t)}{\mu}\right)\cdot\frac{1}{44} \tag{11}$$

The following section presents the data and methods used to investigate the impact of six major factors influencing the K_E. Those factors are 1—Vehicular type, 2—Proportion of

heavy vehicles in fleet distribution, 3—Driver's behavior, 4—Road gradient, 5—Cruising speed, and 6—Wind effect. We note here that the factors investigated in this study are not exclusive. They were primarily selected because they can be feasibly modeled in relevant simulation models (e.g., Vissim and CMEM), as explained in the following section.

4. Data and Methods

This study adopts a four-step sequential method that starts with designing a full-factorial experiment to generate all possible scenarios for the combined impact of all studied factors on the K_E. The next step was to model a test-bed intersection in Vissim. Subsequently, a Vissim-Python-CMEM interface was developed to ensure proper representation of both the dynamics and kinematics elements of the designed scenarios. Finally, the K_E was computed for each investigated emission criterion and all performed scenarios.

4.1. Full-Factorial Experiment Design

We designed a full-factorial experiment [55] to create scenarios for various operating conditions and studied their combined effect on the K_E. The levels of the various investigated factors were chosen in such a way to ensure the diversity of the operating conditions, such as vehicle type, road gradient, speed limit, etc., as detailed in Table 4. Regarding vehicle types, we included 12 Light-duty vehicles (LDVs) and 3 Heavy-duty diesel vehicles (HDDVs) in the experiments. Those 15 vehicle types are out of 31 types available in CMEM and were chosen because they form the largest percentage of the entire vehicle fleet used to develop the CMEM. The first column in Table 4 shows the category number of the selected vehicle groups as they have been named in CMEM (and in this study). It is worth mentioning that the CMEM was developed using vehicles made in the years 1990–2000. CMEM developers have chosen the vehicle/technology categories based on a vehicle's emissions contribution. The emissions standards used to categorize the tested vehicles are the "California Vehicle Emissions Standards" [56]. We note here that LDV1-LDV11 are powered by gasoline, whereas LDV12 and HDDV1–HDDV3 are powered by diesel.

Percentages range between 0% and 10%, with an increment of 1% of heavy vehicles in the fleet, were considered. Following the general recommendations for maximum grades [57], we adopted a road gradient range between −7% and 7%. Cruising speeds (represented by speed limits) usually range from 20 to 65 mph, depending on the geometrical and traffic conditions. Thus, 10 speed limits, with an increment of 5 mph, were chosen to cover all possible speed limits between 20 and 65 mph. The aerodynamic effects were represented by various wind speeds and directions (headwind (HW) and tailwind (TW)). The wind speeds range from zero-wind to a wind of 50 mph, with an increment of 10 mph, for both HWs and TWs. This study only considers the impact of wind on K_E of HDDVs because the wind effect is most profound for trucks, and CMEM does not model the wind effect for LDVs. Finally, the impact of the driver's aggressiveness on K_E is investigated by analyzing four acceleration–deceleration functions, where each function represents a single unique driving behavior. More details about the tested driving-behavior functions are provided later.

A total of 27,000 scenarios have been generated representing all possible combinations of the independent factors impacting K_E for the range of values of each factor given in Table 4. The exception is the fleet distribution, which was investigated by utilizing Equation (12) that computes the K_E for a movement as the sum of the percentage (p) of each vehicle type (i) multiplied by its relevant average stop penalty (K_{Ei}) for all vehicles of type n. It is worth noting that investigating the impact of multiple vehicle types from the same class is out of this study's scope. Thus, LDV1 and HDDV1 are selected to investigate the impact of fleet distribution on the K_E. For LDVs, a total of 7200 experiments were designed (12 (vehicle types) × 4 (driving behaviors) × 15 (grades) × 10 (cruising speeds)). For HDDVs, a total of 19,800 experiments were designed (3 (vehicle types) × 4 (driving behaviors) × 15 (grades) × 10 (cruising speeds) × 11 (wind effects)). Lastly, using the results of the 13,200 experiments, Equation (12) was applied to investigate the impact of fleet distribution on the

K_E. Those 13,200 experiments represent the impact of 11 fleet distributions times (1 (LDV) × 4 (driving behaviors) × 15 (grades) × 10 (cruising speeds) + 1 (HDDV) × 4 (driving behaviors) × 15 (grades) × 10 (cruising speeds)).

$$K_E = \sum_{i=1}^{n} p_i \cdot K_{Ei} \quad (12)$$

Table 4. Levels for various operational conditions impacting K_E.

Vehicle Type		Fleet Distribution	Driver Behavior	Road Gradient	Cruising Speed	Wind Effect
CMEM	This study	LDV:HDDV	Acceleration functions	(%)	(mph)	(mph direction)
Car, Category 1	LDV1	100:0	Function 1	−7	20	50 tailwind
Car, Category 2	LDV2	99:1	Function 2	−6	25	40 tailwind
Car, Category 3	LDV3	98:2	Function 3	−5	30	30 tailwind
Car, Category 4	LDV4	97:3	Function 4	−4	35	20 tailwind
Car, Category 5	LDV5	96:4		−3	40	10 tailwind
Car, Category 6	LDV6	95:5		−2	45	No wind
Car, Category 7	LDV7	94:6		−1	50	10 headwind
Car, Category 8	LDV8	93:7		0	55	20 headwind
Car, Category 9	LDV9	92:8		1	60	30 headwind
Car, Category 10	LDV10	91:9		2	65	40 headwind
Car, Category 11	LDV11	90:10		3		50 headwind
Car, Category 12	LDV12			4		
Truck, Category 5	HDDV1			5		
Truck, Category 6	HDDV2			6		
Truck, Category 7	HDDV3			7		

4.2. Traffic and Emissions Models

Certainly, the best way to measure the impact of various operating conditions on the K_E is through field experimentation and data collection. However, collecting real-world emissions data across all ranges of factors is a challenging and very costly task. A massive dataset is needed to include all possible combinations of factors affecting stop-related emissions and their relevant stop penalties. Therefore, our study is primarily based on simulation experiments, aiming to mimic the real-world vehicular stopping mechanisms under all the possible scenarios, as explained in the following sections.

4.2.1. Traffic Simulation Program

PTV Vissim [52] is a microscopic model developed to simulate urban traffic and public transport operations. Vissim is a popular tool in the traffic community because it is easy to use and can simulate and test almost any traffic-related scenario before being implemented in the field. In addition to the previous advantages, we selected Vissim in this study for the following reasons: 1—Its ability to accurately model traffic signals and other operations (e.g., speed and acceleration) at a resolution of 1 s, 2—It provides the possibilities to model all of the investigated factors in this study (e.g., road gradient per link and driving behavior), 3—Vissim can be easily interfaced with relevant programming languages (e.g., Python), allowing the user to manipulate the investigated factors' attributes and perform many experiments efficiently, and 4—Vissim outputs vehicle trajectory (also known as floating car data) files (FZP), which are well fitted for modeling in CMEM to obtain second-by-second emission estimates.

4.2.2. Modal Emission Model

CMEM [54] is a power-demand emissions model that estimates second-by-second fuel consumption and emissions (HC, CO, NOx, and CO_2) based on vehicular speed and acceleration traces. The developers of CMEM used more than 300 tested vehicles to develop

the model. CMEM has one estimation module for LDVs and another for HDDVs; thus, a user needs to separate vehicles in the fleet before processing their trajectories in CMEM into LDVs and HDDVs. A second-by-second speed trace is required at minimum as an input for CMEM to estimate various emissions, where those inputs can be acquired from Vissim. CMEM was selected for this study for three reasons: 1—CMEM can estimate emissions for various vehicle types, 2—It allows users to include the influence of road gradient (for all vehicle classes) and wind effect (for HDDVs only) on emissions estimates, and 3—CMEM has already been calibrated and validated using data from the National Cooperative Highway Research Program [58]. Moreover, a few studies have already validated estimates from CMEM, and they concluded that CMEM is a generally accepted model that can generate verifiable emissions estimates [59,60]. Therefore, no calibration or validation efforts were needed to perform this study.

4.3. Modeling of a Test-Bed Intersection

We selected a four-leg intersection, IL-21 in Washington Street in Lake County, Chicago, IL, to apply our modeling scenarios for the sake of this study. The intersection has four traffic lanes (two through and one exclusive for each of the right and left turns) at each approach. The Division of Traffic at Lake County, in the Chicago metro area, provided the directional volumes and turning movement counts for the modeled intersection (Figure 3). An eight-phase fixed-time signal timing plan was operated on the simulated intersection. A cycle length of 140 s was modeled, as shown in the Ring-Barrier Diagram in Figure 3. The simulation time was 1100 s, including 200 s for warmup time. This simulation time is long enough to gather relevant results for a minimum of 400 stopped vehicles at the intersection in each performed scenario, representing a sufficient statistical sample size.

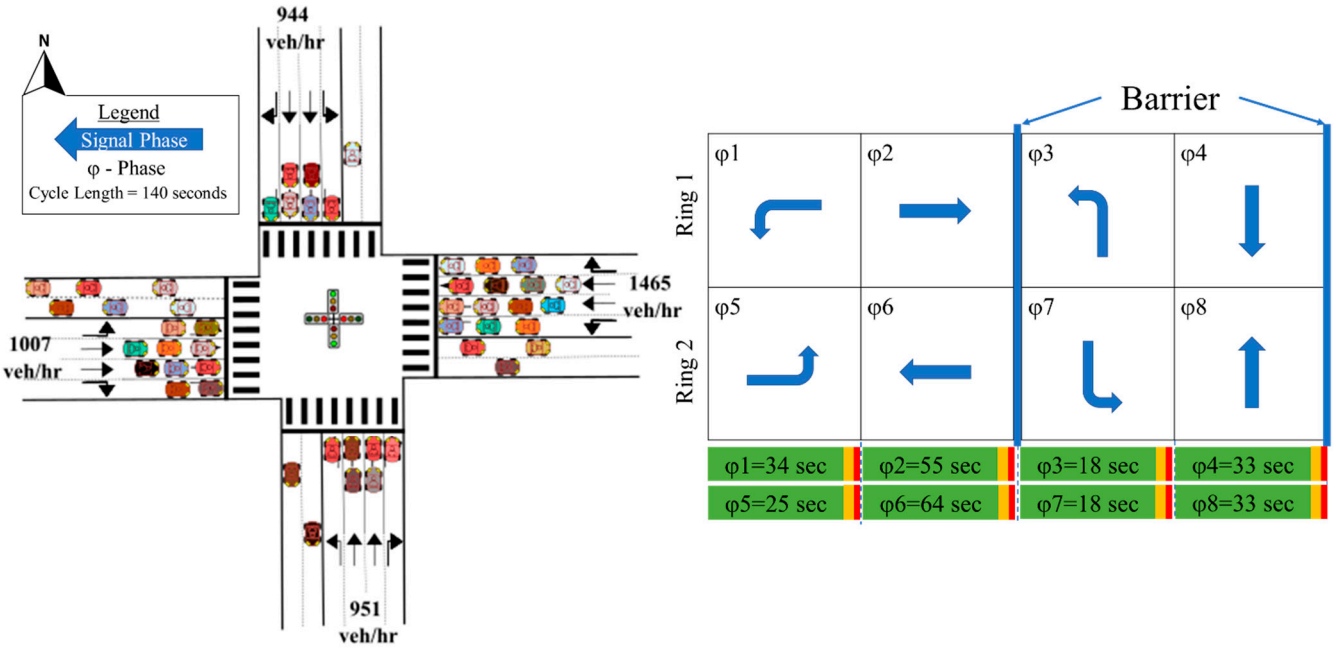

Figure 3. Layout, volumes, and splits of the modeled intersection.

4.4. Modeling of Various Operating Conditions

All the investigated factors, except the impact of wind, were modeled in Vissim and CMEM, whereas the wind effect was modeled only in CMEM. For the vehicle type, two-vehicle classes were modeled in Vissim; cars and heavy goods vehicles (HGVs), which were modeled as LDVs and HDDVs in CMEM. The percentages of cars and HGVs in Vissim were modeled by changing the relative flow value of each vehicle class in the vehicle compositions defined for each intersection approach.

Vissim models cruising speeds by using stochastic desired speed distributions, which assigns the proportion of the vehicles in the fleet that drive higher, lower, and in between the defined minimum and maximum speeds. However, the goal of modeling cruising speeds in this study was to ensure that all stopped vehicles decelerate from a particular speed and then accelerate back to the same original speed. Thus, we defined ten deterministic speed distributions in Vissim for the speeds from 20 to 65 mph with 5-mph steps. Deterministic speed distributions were modeled by setting relative values to each distribution's minimum and maximum speeds. For example, minimum and maximum speeds of 24.99 mph and 25 mph are set to obtain a 25-mph cruising speed before and after stopping for all stopped vehicles. CMEM then uses second-by-second speeds from trajectories to estimate emissions.

Modeling road gradient was done in Vissim to cover the impact on the acceleration and then in CMEM to consider the influence of increased power demand on the emissions estimates. Investigated grades were defined as percentages (e.g., −2% and 2%) for each link in Vissim, starting from the stop line to the point where vehicles reach their original cruising speeds. Afterward, the road gradients (expressed in degrees and radians, respectively, for LDVs and HDDVs) were added to the trajectories from Vissim before further processing in CMEM.

CMEM supports defining headwind and tailwind directions for various speeds on the trajectories processed in the HDDVs module only. Thus, the obtained HGV stop profiles from Vissim were assigned a wind direction and speed according to the performed scenario. Finally, the driving behaviors investigated in this study were represented by various desired deceleration–accelerations functions, as explained in the following subsection.

4.5. Modeling of Driving Behaviors

The desired acceleration or deceleration value assigned to vehicles at each time step in the simulation is one of the most critical and relevant elements to determine driver behavior in Vissim [52]. Vissim defines acceleration and deceleration values (referred to as acceleration–deceleration functions hereafter) as functions of the current speed. Both acceleration–deceleration functions consist of three curves representing the minimum, median, and maximum possible acceleration–deceleration values at different speeds [52]. Although Vissim provides default acceleration–deceleration functions for various vehicle classes, utilizing those functions is problematic from two aspects. First, the default acceleration–deceleration functions in VISSIM are based on an older dataset from Europe [52]. Consequently, a few studies [61,62] indicated that such functions do not apply to current fleets in the US. Second, the acceleration–deceleration functions in Vissim are stochastic because the acceleration or deceleration value, at a certain speed, lies within a specific range between the minimum and maximum values. That means that each stopped vehicle in the simulation can have a unique driving behavior, making it impossible to capture the impact of deceleration–acceleration functions (driving behaviors) on the K_E. Moreover, using stochastic functions adds noise to the results of the impact of the other factors.

Two actions were taken to overcome the issues emerging from using Vissim's default acceleration–deceleration functions. First, we used a vehicular trajectories dataset of 177 vehicles, including 1850 h of driving and more than 40,000 traveled miles, to develop a set of acceleration–deceleration functions representative of the US fleet. Second, we utilized the Dynamic Time Warping (DTW) [63] and k-means clustering [64] algorithms to classify the newly developed stochastic acceleration–deceleration functions into four deterministic functions utilizing a relatively large sample of stopped vehicles. Such deterministic functions enable fully controllable experiments, which guarantee accurate quantifying of the impact of various driving behaviors and other factors (e.g., cruising speed) on the K_E factor.

4.5.1. Developing Field-Based Acceleration–Deceleration Functions

The dataset used to develop the acceleration–deceleration functions was collected by the Idaho National Lab [65] for the Department of Energy [66]. The dataset was retrieved

from field driving runs conducted on various urban arterials in Michigan under different operating conditions. This study used the high-resolution (up to 0.1 s) speed data recorded in the dataset to compute second-by-second acceleration–deceleration values at different speeds. The computed acceleration–deceleration values were distributed to a speed range from 0 to 140 mph with an increment of 10 mph, as shown in Figure 4. When developing the curves in Figure 4, we noticed that the maximum and minimum acceleration–deceleration values at different speeds are extreme values and rarely occurred on few occasions. Hence, such extreme values cannot be generalized and used for an entire simulated fleet. Thus, the maximum and minimum curves are not the ultimate maximum and minimum; instead, we prepared the curves by computing the averages of the maximum and minimum 20% of the acceleration–deceleration values at various speeds. The next step was to use such stochastic functions retrieved from the field data to generate deterministic driving behavior functions.

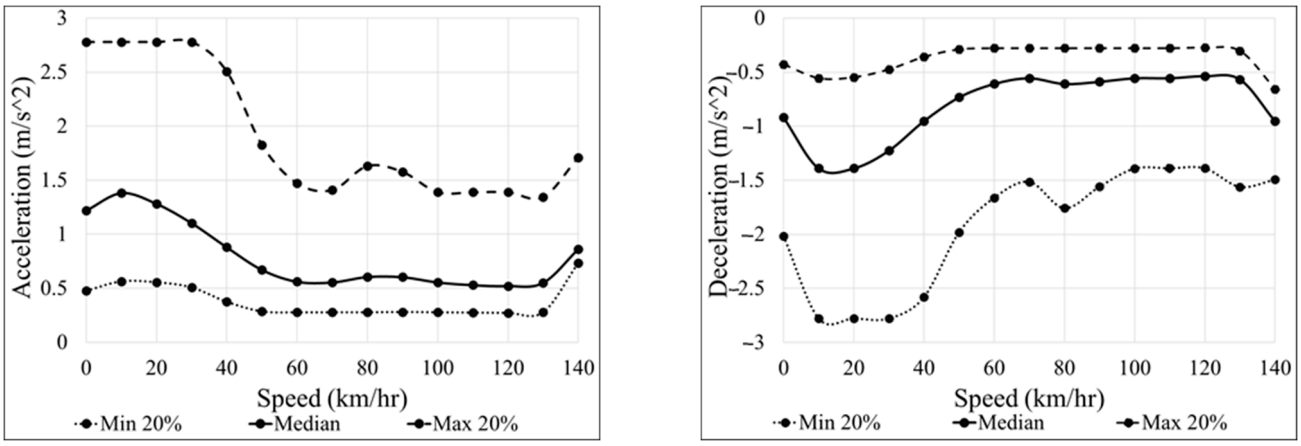

(**a**) Desired acceleration function (**b**) Desired deceleration function

Figure 4. Desired acceleration–deceleration functions developed using vehicular field trajectories.

4.5.2. Generating Deterministic Driving Behaviors

As mentioned previously, using stochastic acceleration–deceleration functions create many driving behaviors within a single tested scenario, defeating the purpose of the study's investigation. This issue was alleviated by conducting a simulation run on the modeled test-bed intersection to obtain a large sample of deterministic acceleration–deceleration functions for individual stopped vehicles in the simulation. Then, the acceleration–deceleration functions of those stopped vehicles were extracted from Vissim and compared internally by using the DTW algorithm. This algorithm provided a dissimilarity score between every acceleration–deceleration function and all the other functions. Finally, such dissimilarity scores were fed into the k-means clustering algorithm to group all acceleration–deceleration functions into an optimal number of groups. Nominal operating conditions were modeled for this simulation run (e.g., level-terrain and acceleration–deceleration functions in Figure 4) except for the speed, which was selected to be 60 mph. The reason for choosing 60 mph is that the time taken by a vehicle to accelerate from 0 to 60 mph is a commonly used performance measure for vehicle acceleration [67]. The simulation run resulted in over 400 stopped vehicles, which were used in the process described in Figure 5.

The comparison of two time series (e.g., deterministic acceleration–deceleration functions) is usually made by producing a distance metric between every two points that coincide in the two input time series (Figure 6a). As a result, such a distance is not appropriate for comparing deterministic acceleration–deceleration functions because they vary in length. Thus, the DTW algorithm was used because it applies a non-linear (elastic) alignment through time-normalization for distances between points in two data series (Figure 6b) [63]. In this way, the pattern match is recognized between two similar time intervals even if they do not have the same length.

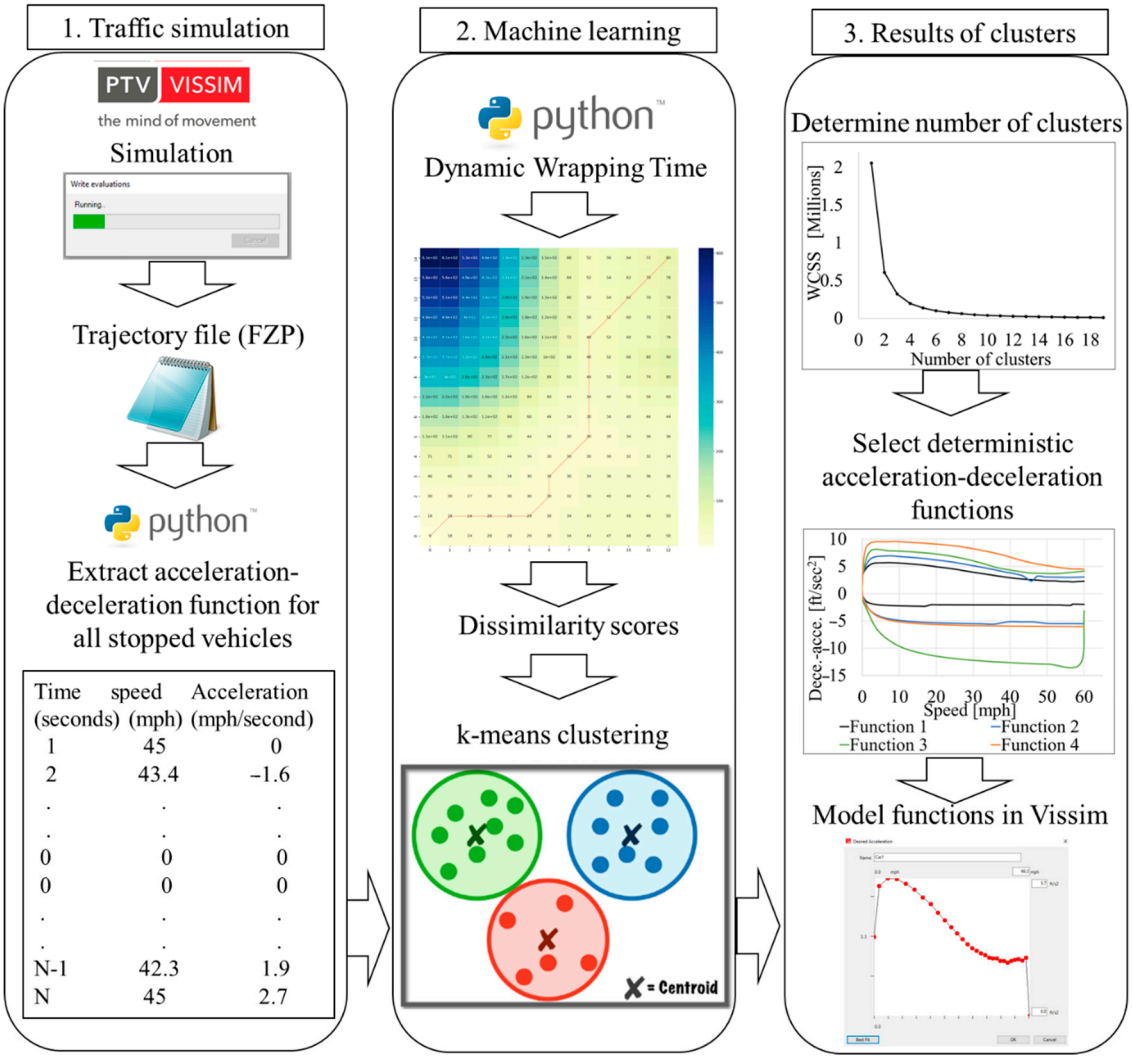

Figure 5. Clustering stochastic driving behaviors into deterministic groups.

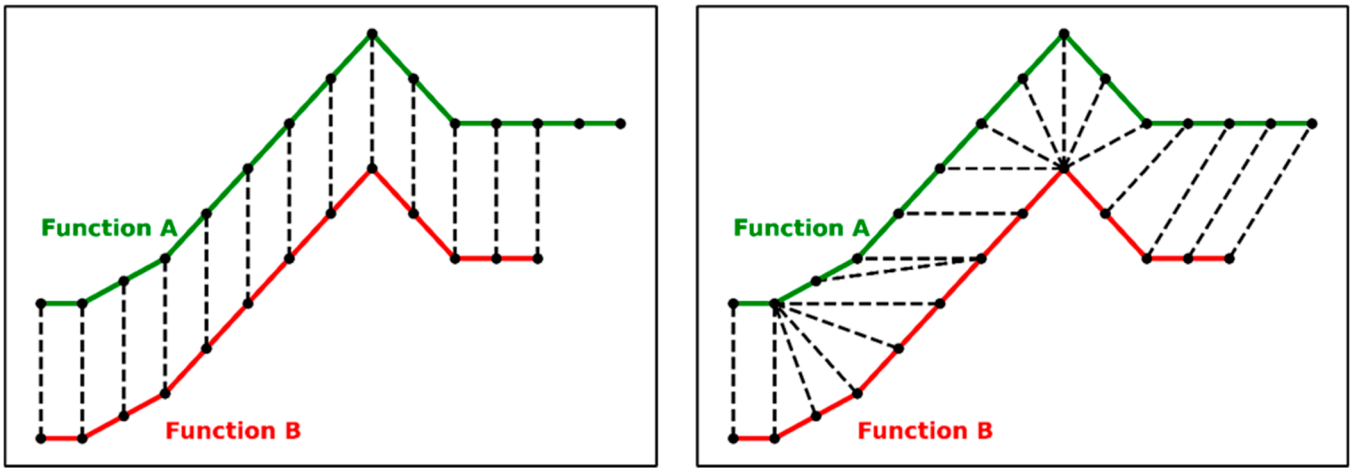

(**a**) Regular comparison (**b**) DTW algorithm comparison

Figure 6. Difference between linear and elastic alignments when comparing two time series.

The following is an overview of the DTW and k-means algorithms. Acceleration–deceleration functions in Figure 6 can be expressed as a sequence of feature vectors A and B.

$$A = a1,\ a2, - - -,\ a_x, - - -, a_X B = b1,\ b2, - - -,\ b_y, - - -, b_Y \tag{13}$$

Using the aid of an x-y plane, shown in Figure 7, where A and B sequences are developed along the x and y-axes, respectively. The timing differences between A and B can be depicted by a sequence of points $\Delta t = (x, y)$:

$$F = \Delta t(1),\ \Delta t(2), - - -,\ \Delta t(k), - - -, \Delta t(K) \tag{14}$$

where: $\Delta t(k) = (x(k), y(k))$, k: any point in sequence F, K: number of points in sequence F.

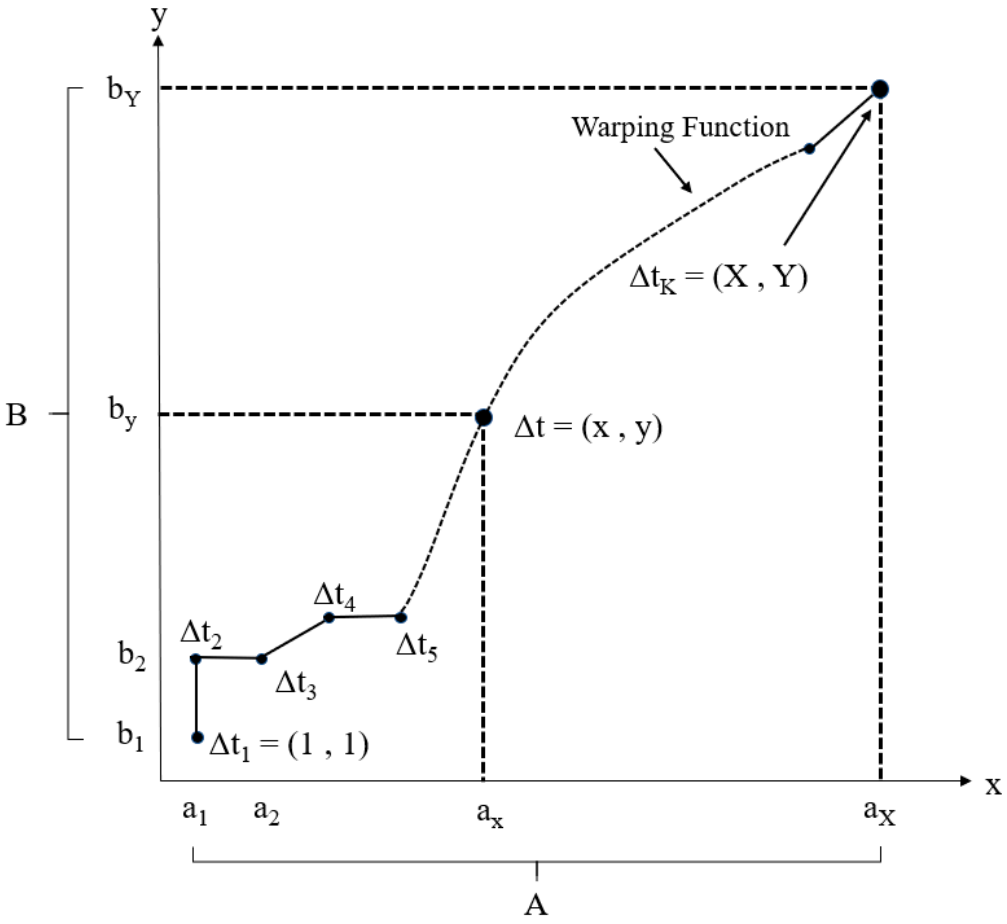

Figure 7. Representation of a typical DTW programming algorithm.

Sequence F can represent a function that creates a mapping from the time axis of function A to function B, which is called a wrapping function (F). This function coincides with the diagonal function x = y when the difference in time between A and B is zero, whereas it shifts further up or down as the time difference grows. Distance d can be used as a measure of the difference between any two points a_x and b_y as follows:

$$d(\Delta t) = d(x, y) = ||a_x - b_y|| \tag{15}$$

Then, the weighted summation of distances on the function F is expressed as:

$$E(F) = \sum_{k=1}^{K} d(\Delta t(k)) \cdot w(k) \tag{16}$$

where: $w(k)$ is a non-negative weighting coefficient introduced to allow $E(F)$ to measure flexible features on the compared time series and measure the goodness of the function F [63]. The dissimilarity score (D) is then defined as the distance between functions A and B after eliminating time differences between them, as shown in Equation (17), where $w(k)$ in the denominator is utilized to compensate for the effect of the number of points (K). In conclusion, a lower dissimilarity score means the series is more similar.

$$D(A,\ B) = Min_F \left[\frac{\sum_{k=1}^{K} d(\Delta t(k)) \cdot w(k)}{\sum_{k=1}^{K} w(k)} \right] \tag{17}$$

Once the dissimilarity scores between all the deceleration-acceleration functions from the 400 stopped vehicles were computed, the widely used k-means clustering algorithm was then applied to the unique values of the dissimilarity scores aiming to divide them into k similar groups. The clustering was done such that changing the cluster of any dissimilarity score will not minimize the Within-Cluster Sum of Squares (WCSS) [64]:

$$WCSS = arg_S\ min \sum_{i=1}^{m} \sum_{x=1}^{n} ||x - \mu_i||^2 \tag{18}$$

where: μ_i is the averages of dissimilarity scores contained within cluster i (i = 1, 2, . . . , m), and n is the number of dissimilarity scores in cluster i.

The next step was to determine the optimum number of clusters by using the heuristic Elbow method, which requires the following steps: 1—Perform k-means clustering for n number of clusters, 2—Compute WCSS for each clustering result, 3—Graph the WCSS (y-axis) and the number of clusters (x-axis) as introduced by Thorndike [68], and 4—Determine the optimum number of clusters at which a point marks a sudden flattening of the curve. This point on the curve suggests that using more clusters is no longer worth the decrease in WCSS. According to the Elbow method chart (Figure 8a), four clusters were selected to be the optimal number of clusters. Figure 8b presents the four selected deterministic acceleration–deceleration functions. The deceleration and acceleration of the selected functions from 60 to 0 mph and from 0 to 60 mph, respectively, are as follows: (−1.92, 3.4), (−4.4, 4.2), (−7.35, 4.9), and (−4.65, 6.3) for function 1, function 2, function 3, and function 4, respectively, all units in ft/sec^2. The final step was to model those functions in Vissim as desired acceleration–deceleration functions.

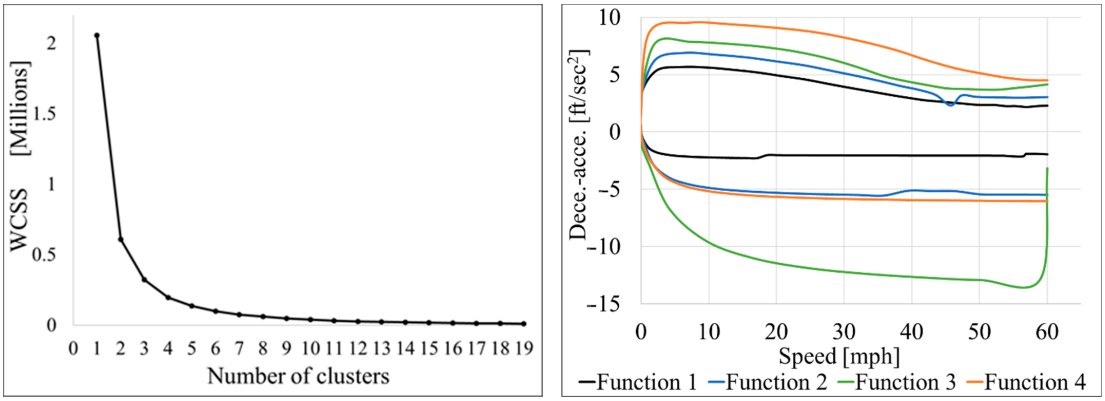

(**a**) The optimal number of clusters (**b**) Acceleration–deceleration functions

Figure 8. Results of k-means algorithm.

4.6. Vissim–Python–CMEM Interface

This section focuses on the interfaces formed among Vissim, Python, and CMEM. A robust code developed in Python controls Vissim externally and connects Vissim with the LDV and HDDV modules in CMEM (Figure 9). The code starts with a for-loop to iterate the

investigated operating factors in Vissim based on the scenario to be performed. The code then runs the simulation in Vissim, which provides simulation time, a vehicle identifier, a vehicle type (LDV or HDDV), speed, acceleration or deceleration, and the number of stops on a second-by-second basis. The Python interface code uses Vissim's vehicular trajectories to extract stop profiles for all stopped vehicles. Following this, the code formats stop profiles to be processed in CMEM and assigns a CMEM-based vehicle category to the LDVs and HDDVs. The code then calls the LDV or HDDV module in CMEM for each vehicle through the command prompt. CMEM uses individual vehicle data to estimate instantaneous emissions for each vehicle. Next, the code computes the emissions-based stop penalty for each emission type for each stop profile. Finally, the average stop penalty for each emission type is calculated for each scenario.

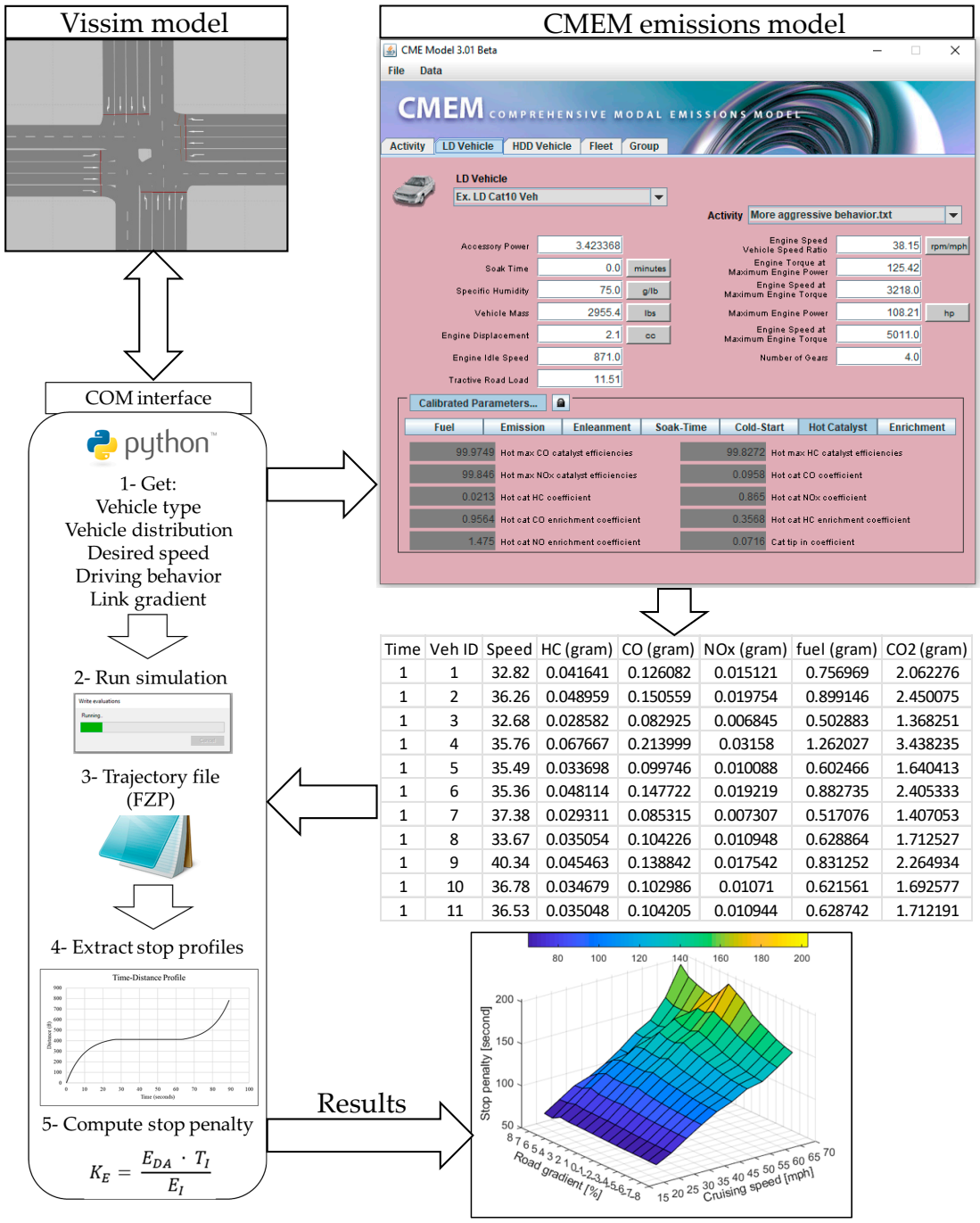

Figure 9. Vissim–Python–CMEM integration.

5. Results

Figure 10 shows the individual impact of the tested factors on the K_E to assess how each of the tested factors impacts the K_E.

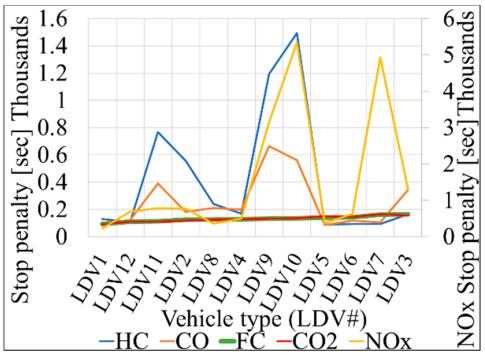

(**a**) LDV type vs. stop penalty

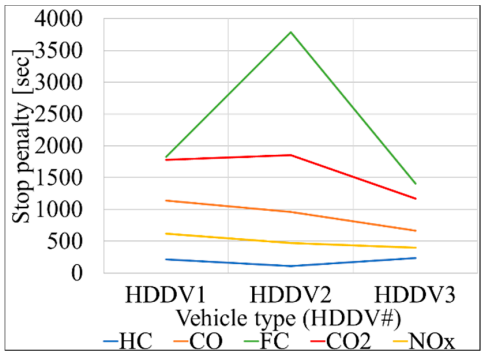

(**b**) HDDV type vs. stop penalty

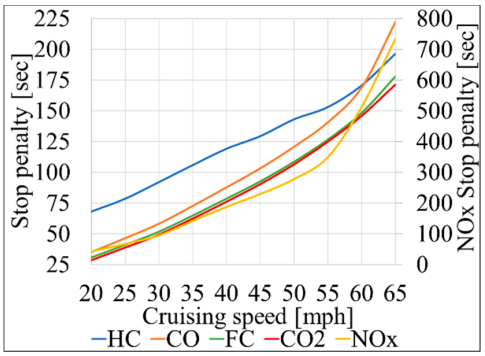

(**c**) Cruising speed vs. stop penalty for LDV

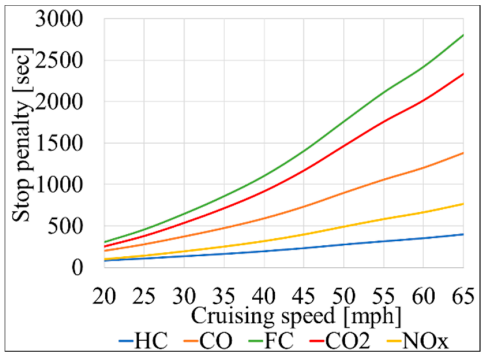

(**d**) Cruising speed vs. stop penalty for HDDV

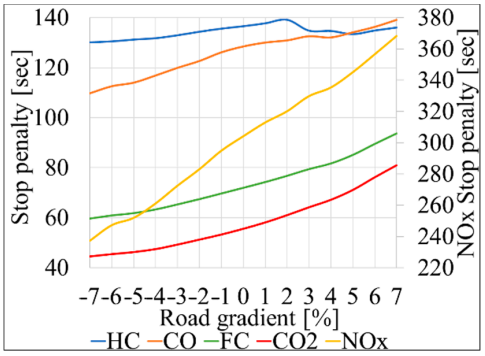

(**e**) Road gradient vs. stop penalty for LDV

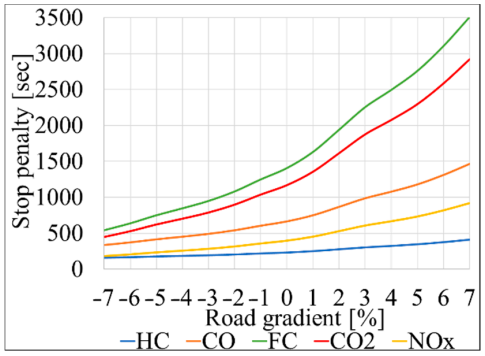

(**f**) Road gradient vs. stop penalty for HDDV

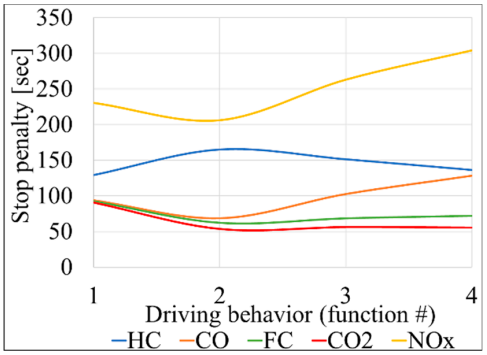

(**g**) Driving behavior vs. stop penalty for LDV

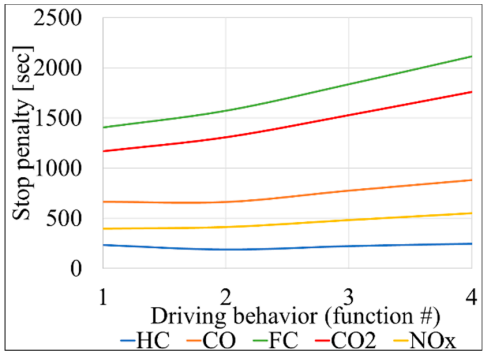

(**h**) Driving behavior vs. stop penalty for HDDV

Figure 10. Individual impact of several independent factors on the stop penalty.

The left part of Figure 10a,c,e,g presents the individual impact of various LDVs, speeds, grades, and driving behavior on the K_E of different emission types and fuel consumption. Similarly, the right part of Figure 10b,d,f,h shows the impact of the aforementioned factors on the K_E for the HDDVs. The individual impact was determined by varying one factor while keeping all other factors constant. It is apparent from Figure 10 that the K_E of the HDDVs is ~3–10 times large than that of the LDVs. These experimental results provide apparent evidence that various emission criteria are not necessarily linearly correlated. Thus, minimizing a particular criterion does not necessarily minimize others. This conclusion is expected [20] and suggests that a unique value of the stop penalty is required to minimize each emission criterion. For example, for a movement with a road gradient of 2%, a K_E value of 139, 130, 76, 61, and 320 s is required to minimize HC, CO, FC, CO_2, and NOx, respectively. A careful analysis of these values could help us define signal optimization strategies for various cities based on their sensitivity to a particular emission type.

The individual impact of wind speed and direction and the percentage of heavy vehicles in the fleet are shown in Figure 11. We can see from Figure 11a that wind solely has a significant impact on the KE, especially at high headwind speeds (>20 mph). That is because the wind direction and speed directly impact the effective speed of a moving vehicle. Thus, an accelerating vehicle upwind/downwind produces more/less fuel consumption and emissions than an accelerating vehicle with no wind conditions.

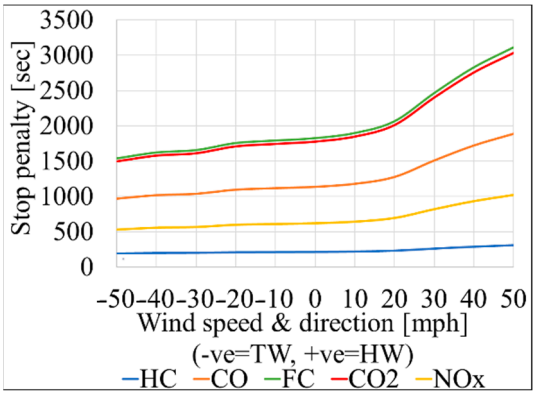

(**a**) Wind vs. stop penalty

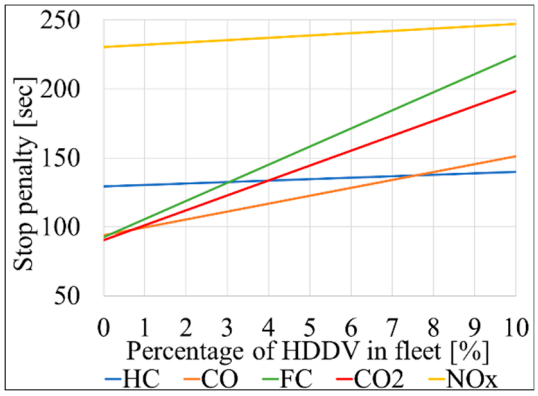

(**b**) % HDDVs in fleet vs. stop penalty

Figure 11. Individual impact of wind effect and percentage of heavy vehicles on the stop penalty.

The results in Figures 10 and 11 prove the importance of the combined effect of different operating conditions on the K_E. The combined impact of multiple factors on the K_E is visualized by using the 3D plots in Figure 12 to depict several relationships between the independent factors and the K_E. The plots shown in Figure 12 are based on the results of LDVs. The same patterns for all the plots can be seen from the results of HDDVs (not shown in the paper, for brevity). Each plot presents the fluctuation in the K_E of a particulate emission criterion (E) at a bivariate level, meaning that only two parameters are varied. At the same time, all other factors were fixed at their nominal values. Those values are LDV1, level-terrain, 45-mph speed, and acceleration–deceleration function 1. For example, Figure 12a shows a significant change in the K_{HC} with the increase of cruising speed and road gradient for LDV1 and the driving behavior function 1. Although the other emission criteria (not shown in the paper) follow a similar relationship between speed, grade, and stop penalty as the one shown for the HC, the magnitude of the K_E is unique (higher or lower) for each criterion.

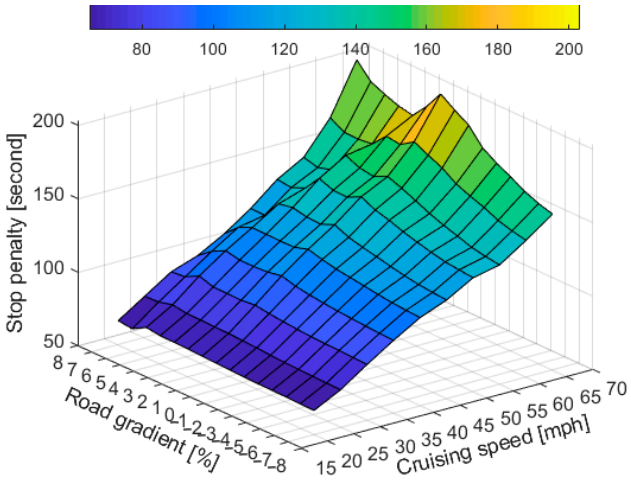

(**a**) Cruising speed and road gradient vs. K_{HC}

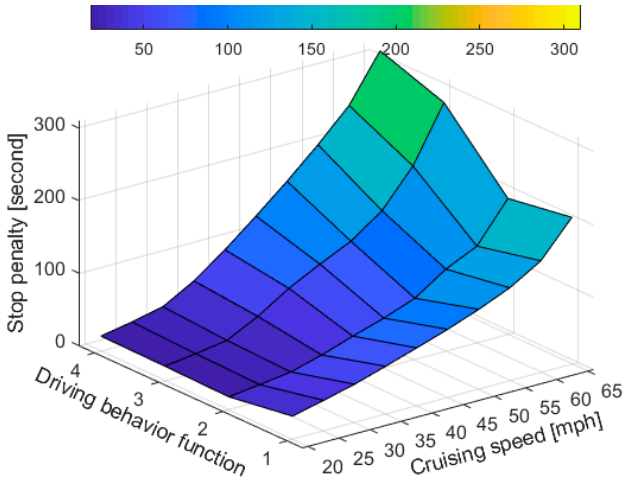

(**b**) Cruising speed and driver behavior vs. K_{CO}

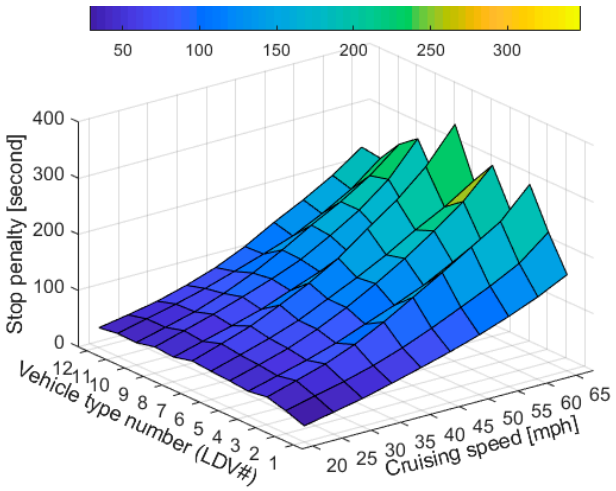

(**c**) Cruising speed and vehicle type vs. K_{CO2}

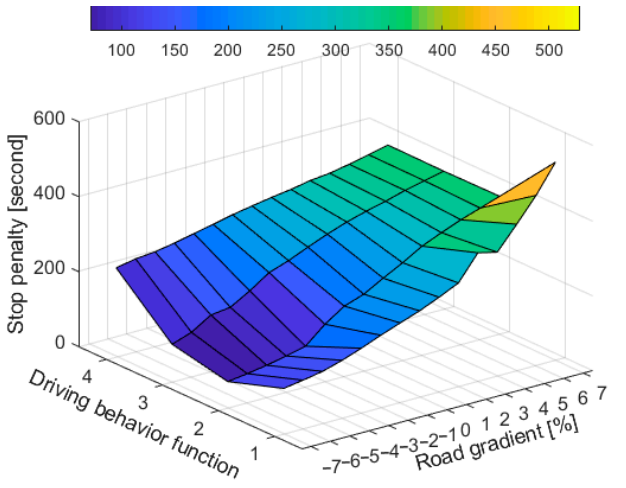

(**d**) Road gradient and driver behavior vs. K_{NOx}

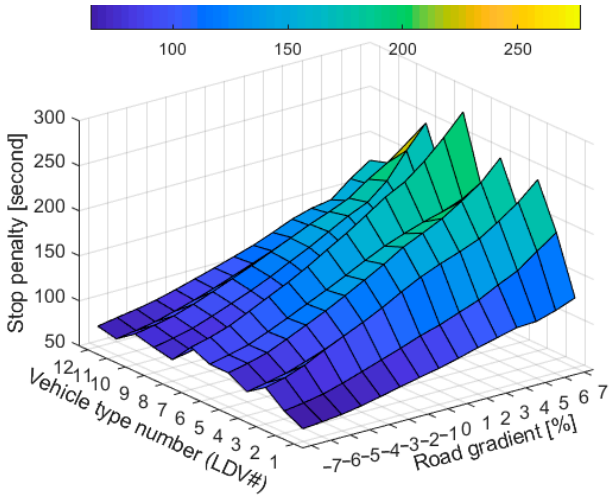

(**e**) Road gradient and vehicle type vs. K_{CO2}

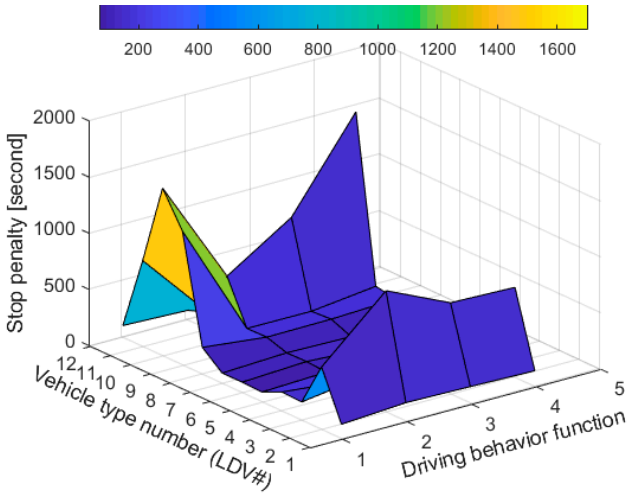

(**f**) Driver behavior and vehicle type vs. K_{HC}

Figure 12. Relationships between stop penalty and its independent factors for various emissions.

Figures 12 and 13 present representative results of the impact of the wind effect and the percentage of heavy vehicles in the fleet on the K_E under various cruising speeds and

road gradients. As mentioned in previous sections, our analysis investigated the impact of wind effect only for the HDDVs; hence Figure 13a,b presents the change in the K_E of an HDDV. As expected, the wind speed and direction have shown that headwinds cause the HDDV to utilize more energy (which produces more fuel consumption and emissions) to overcome the wind blowing in the opposite direction. The findings in Figure 13c,d confirm a significant positive correlation between the percentage of HDDVs in the fleet and the K_E. Such a correlation becomes even more apparent under extremely high and low cruising speeds and grades.

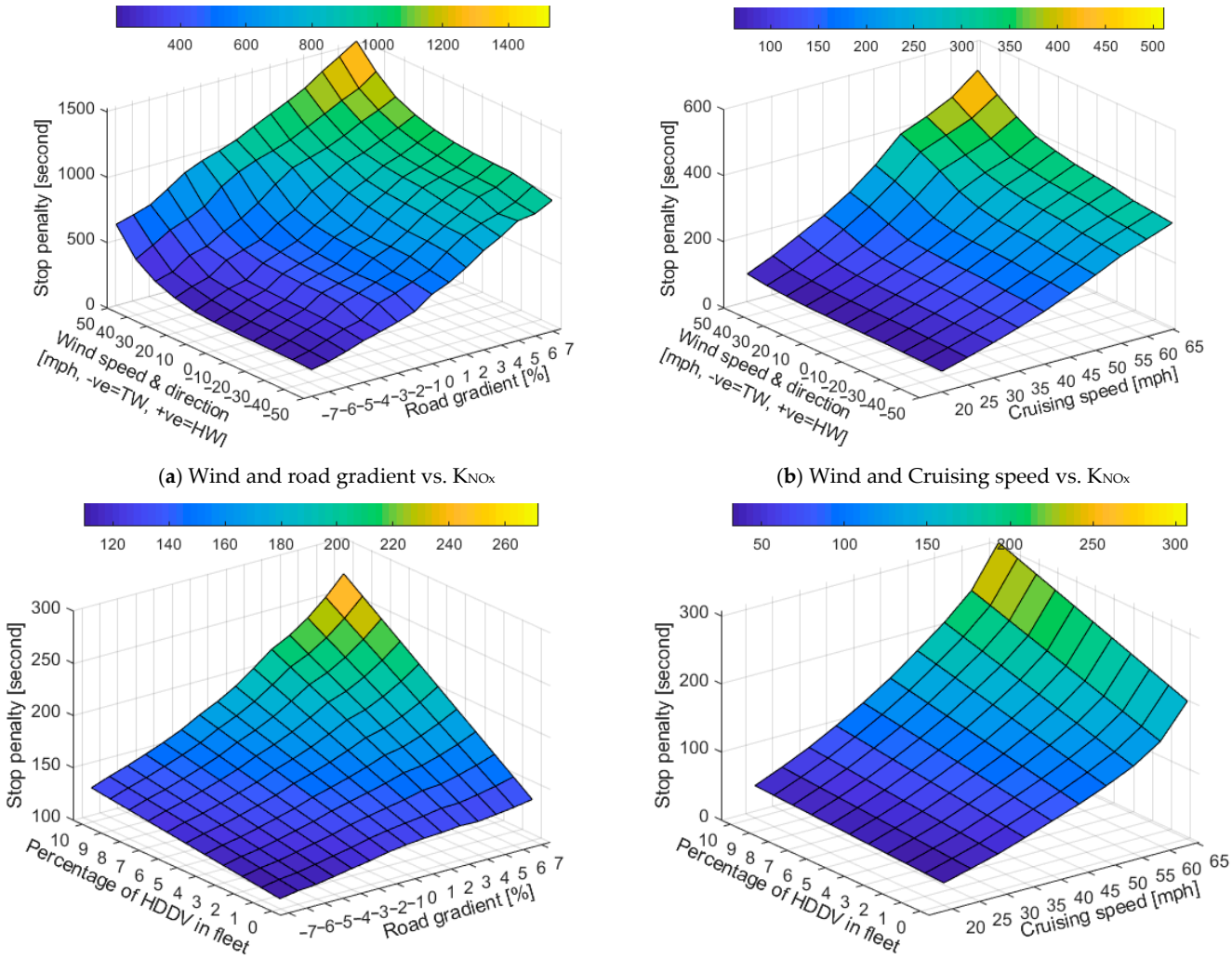

(**a**) Wind and road gradient vs. K_{NOx}

(**b**) Wind and Cruising speed vs. K_{NOx}

(**c**) %HDDV in fleet and road gradient vs. K_{CO}

(**d**) %HDDV in fleet and Cruising speed vs. K_{CO}

Figure 13. Relationships between stop penalty and its independent factors for various emissions.

The impact of the percentage of HDDVs on the K_E (shown in Figure 11b) suggests that the combined impact of this percentage with multiple factors will have a significant impact on the K_E. The impact is depicted in Figure 13c,d, and it is logical because LDVs and HDDVs have different engine sizes and technologies, which leads to various production rates of fuel consumption and emissions. The following section discusses the relationship between each factor and the K_E.

6. Discussions

Based on the ranges of the stop penalty, resulting from various factors shown in Figure 10, the main parameter that drives the K_E values (of various emission criteria) is

the vehicle type. The impact of vehicle type does not seem to follow an easily identifiable pattern. On one side, the minimum K_{HC} and K_{CO} belong to normal emitting LDV (three-way catalyst, fuel-injected, >50K miles, high power/weight ratio), as shown in Figure 10a. In contrast, the minimum K_{NOx}, K_{FC}, and K_{CO2} belong to normal emitting LDVs with no catalyst. Similarly, the maximum K_E of different emission criteria belongs to various vehicle types. Moreover, the K_{HC} and K_{CO} of some vehicles increase or remain constant with the decrease of K_{NOx}, K_{FC}, and K_{CO2}. Thus, it seems that reducing FC and CO_2, as generally adopted practices in the traffic community, may not lead to a tangible reduction in HC and CO. Previous studies have not recognized this inconsistency in the results. That can be explained, at least partially, by the different vehicle masses, engine powers, fuel used per engine's displacement, engine efficiency, and engine technologies used by vehicle manufacturers.

A question may arise concerning the high values of the K_{HC} and K_{NOx} for LDV 7, 9, 10, and 11, as shown in Figure 10a. The reason for such high values is the occasionally low emitting (approaching zero) CMEM's CO and NOx estimates, for those LDV types, during idling. These low emitting values significantly increase the K_E, according to Equation (7). However, it is not clear why CMEM resulted in such low estimates.

Figure 10b shows how the stop penalty fluctuates for HDDVs. Unexpectedly, it can be seen from Figure 10b that the K_{HC} and K_{NOx} have an inverse relationship with the K_{CO}, K_{FC}, and K_{CO2}. That can be easily seen in the transition in the curves from HDDV1 to HDDV2 and from HDDV2 to HDDV3. K_{CO}, K_{FC}, and K_{CO2} increased in the first transition while K_{HC} and K_{NOx} slightly decreased. The opposite happened in the second transition where K_{CO}, K_{FC}, and K_{CO2} decreased, K_{NOx} barely decreased for HDDV3, but K_{HC} has increased. These are all crucial findings to consider when computing the stop penalty, especially for fleets with a high proportion of heavy vehicles.

Indeed, decelerating and accelerating from/to higher cruising speeds requires more energy and emits more emissions, which explains higher K_E. The cruising speed is the second most significant parameter, and it has a positive exponential relationship with the K_E. This is mainly observed for CO, CO_2, fuel consumption, and at speeds higher than 50 mph, for HC and NOx, as shown in Figure 10c,d.

The observed significant increase in K_E with the increase in speed could be attributed to the cruising speed before or after stopping. These results depend on the emitting rate of a specific emission type during each phase of the stop. For example, Figure 2 shows that HC rates are higher for a specific vehicle type while decelerating, whereas CO_2 rates are the highest during accelerating. That should be a major concern when computing the stop penalty for left and right turn movements, as their cruising speeds before and after stopping are usually significantly different. Keeping in mind that emitting rates during various phases depends on the vehicle type, the impact of cruising speed on the K_E cannot be separated from the impact of the vehicle type.

The emissions generally increase when vehicles travel uphill and combat gravity. On the other hand, potential energy is added to the engine's kinematic energy when traveling downhill; thus, less emissions are produced on downhill terrains. The findings of this study found that the relationship between road gradient and the LDVs K_E can be identified as linear for CO and NOx and second order polynomial for CO_2 and fuel consumption. A linear relationship can also be observed for the HC at grades between −7% and 2% (Figure 10e); however, K_{HC} decreases slightly and does not seem to be impacted by higher grades. That is attributed to the fact that HC estimation while idling is very sensitive to the increased engine load [54]. Thus, resulting in lower K_{HC} variations (between 130 and 140 s) than the other emission criteria.

The impact of road gradient on the HDDVs K_E seems exponential (Figure 10f), with the K_{HC} and K_{FC} being the least and the most sensitive to grade increase, respectively. We note here that the HDDV categories in CMEM are for heavy trucks manufactured in the years between 1995 and 2000; thus, newer trucks may have lower K_E because of the

new legislation released since then concerning reducing emissions. Nevertheless, it is still expected that HDDVs stop penalties will be significantly higher than those for LDVs.

Regarding driving behaviors, the results showed that the levels of accelerations and decelerations significantly impact the K_E. That is a logical and expected finding considering that individual driver's driving habits control the amount of fuel injected into the engine. The impact of driving behavior on the K_E does not follow a recognizable pattern and is not easily predictable, especially for LDVs, as shown in Figure 10g. For example, although function 1 has the lowest acceleration–deceleration values and resulted in the lowest K_{HC} and second-lowest K_{CO}, it also had the highest K_{CO2} and K_{FC}. Interestingly, function 3 has the highest deceleration and resulted in the second-highest stop penalty for all emission types and fuel consumption. Such results indicate the importance of the deceleration phase duration despite the low emitting rate of most of the emission types during that phase. Figure 10h shows that the HDDVs stop penalty under various driving behaviors seemed to follow expected patterns, where the stop penalty increases with more aggressive (higher) accelerations. Such patterns could be seen clearly for K_{CO}, K_{NOx}, K_{FC}, and K_{CO2}. However, a much lower impact is observed for the K_{HC}. We note here that although the stochastic acceleration–deceleration functions developed in this study were based on a large dataset, it is expected that the stop penalty could diversify more with a higher degree of stochasticity in driving behavior. Overall, these results indicate that further research is needed to better understand the impact of driving behavior on the K_E, especially for LDVs.

The results of wind effects have shown that the K_E increases linearly with the decrease of the tailwind speed and the increase of the headwind speed. For example, a 20-mph headwind could increase K_{CO} from 1150 s at no-wind conditions to 1300 s (Figure 11a). This difference is equal to 150 extra seconds of CO production while idling. In the opposite direction, a 20-mph tailwind could decrease K_{CO} by 40 s compared to its value at no-wind conditions. One can conclude that the excess emissions saved from a tailwind of a certain speed cannot recover the emission increases caused by a headwind of the same speed magnitude. We note here that the wind effect is most profound for trucks because of their large drag area against the airflow while moving. That does not mean that wind speed and direction will not impact LDVs stop penalties. However, such impact is left for future research due to the unavailability of emissions models to estimate fuel consumption and emissions under various wind speeds and directions for LDVs.

The impact of the proportion of heavy vehicles in the fleet is significant for most emission types and fuel consumption, as shown in Figure 11b. That finding is expected after observing the significant differences between stop penalties for each of the LDVs and HDDVs. Although the relationship between the percentage of HDDVs and the K_E is linear for all emissions and fuel consumption, the intensity (slope of the line) is noticeably different. The most variation caused by the percentage of heavy vehicles is observed for K_{FC} and K_{CO2}. The K_{CO} and K_{NOx} come in second and third place, respectively, whereas K_{HC} increases intangibly (1 s) with each 1% increase in the percent of HDDVs. These remarkable findings suggest that, on the one hand, reducing the production of CO, CO_2, and fuel consumption of a fleet relies on reducing those parameters from both LDVs and HDDVs. On the other hand, reducing HC and NOx depends much more on controlling those parameters from the LDVs.

Most of the results presented in Figures 10 and 11 confirm that the emitting rate of CO2 is strongly correlated with the fuel consumption rate. Hence their stop penalties are relatively similar under various operational conditions. That suggests that aiming to minimize either of them will minimize the other.

Although deriving the emissions-based stop penalty proposed in this paper is applicable for vehicles with Internal Combustion Engine (ICE), zero-emissions vehicles (electric vehicles) can still be combined with the ICE vehicles in the process of developing or optimizing signal timings plans using the proposed Environmental Performance Index. In such a case, the stop delay and number of stops can be applied similarly to the ICE vehicles. However, the stop penalty can be used as the number of seconds of delay is

equivalent to a stop-event (e.g., a widely used value of 10 s). Future research is needed to derive an energy-based stop penalty to include the impact of stops made by the emerging electrical vehicles.

This study used a simulation-based investigation, the conclusions of which can be applied to any region. However, since the emissions model used in this study is developed based on an American vehicular fleet, the results are highly applicable to the US fleet or any similar fleet. Although it is expected that the same investigation results in other regions would not deviate significantly from the results presented in this paper, we recommend using a relevant emissions model to the area of interest when computing the emissions-based stop penalty.

The findings of this are clear and can be summarized as follows: First, various emission types have different stop penalties; thus, unique Env-PI under the same conditions are in order. Thereby, minimizing a particular emission criterion may decrease but will not necessarily minimize another criterion. The exception is the minimization of fuel consumption which minimizes CO_2 because of their linear correlation. This finding does not support the claims of previous studies [9,14,46,69,70] that reported a reduction of an equal magnitude for all the emissions using the same objective function. Second, various operating conditions have a significant impact on the stop penalty. Thus, the stop penalty required to minimize a specific emission type on a particular link varies based on the link's vehicular, operational, topological, and external parameters. That means a link-based observation of traffic dynamics and geometry should be made if one optimizes signals to reduce emissions. Subsequently, those observations should be used to estimate the stop penalty for a specific emission type to be reduced when optimizing signal timings. We note here that the findings presented in Figures 10–13 are representative of the entire findings of this study. Hence, such figures are not adequate to estimate the K_E under the combined impact of multiple factors for various emission criteria. However, the presented figures can be used to estimate the K_E for the cases and emission types presented in them. Future research efforts to develop predictive models to estimate the K_E under the compound impact of various factors have already begun. Such predictive models are required to estimate the stop penalty under the combined impact of multiple real-world conditions. Once the K_E is estimated from the predictive models, it will be used in the proposed Env-PI objective function (Equation (8)) to minimize sustainability metrics in signal timings optimization procedures. Future research should also include utilizing the Network Fundamental Diagram (NFD) to evaluate the impact of optimal signal plans developed using the Env-PI on the traffic conditions of the signalized corridor of interest, as outlined in [71,72].

7. Conclusions

Reducing emissions by optimizing traffic signals is challenging and requires a lot of work to quantify the various air emission criteria under various signal timing plans. However, reducing one type of emissions does not minimize other emissions, and it is likely to increase the delay. To solve this issue, this study derived an emission type-based environmental objective function (called Env-PI) to minimize particular emission criteria. The paper also explained how the Env-PI is different for various emissions based on the emissions-based stop penalty, even under identical operating conditions. Furthermore, the present study reveals the relationship between various operating conditions and the emissions-based stop penalty.

We generated emissions-based stop penalty data using a set of full-factorial experiments and based on simulated traffic and emissions data. A real-world intersection has been modeled in Vissim to perform various experiments under different operating conditions. Vehicular trajectories from the field were used to develop acceleration–deceleration functions, which were utilized to represent various driving behaviors. The emissions model, CMEM, has been used to estimate the investigated emissions (HC, CO, NOx, and

CO_2) and fuel consumption. A Vissim–Python–CMEM interface has been developed to speed up the experimental work and minimize errors.

The results reveal a significant relationship between the emissions-based stop penalty and the independent parameters, including the vehicle type, percentage of heavy vehicles, driver behavior, road gradient, cruising speed, and wind effect. Furthermore, the findings show that all the investigated independent parameters have a significant individual impact on the emissions-based stop penalty. The main parameters driving the variation in the stop penalty are the vehicle type and cruising speed, while the road gradient and driving behavior had a slightly lower impact.

Furthermore, the emissions-based stop penalty value differs for different emission criteria depending on their emitting rates during each stop's driving phase. Thus, our study concluded that using the Env-PI with an accurate estimation of its stop penalty is vital to minimize emissions through optimizing traffic signals. This is especially true for urban communities suffering from specific polluting criteria, where such an Env-PI can be deployed to develop new signal retiming strategies or integrated into existing ones.

Finally, a few critical limitations need to be considered. First, our study used the same acceleration–deceleration functions for both LDVs and HDDVs due to the lack of HDDVs trajectories from the field. Although this assumption is not perfect, it introduces a smaller error than using Vissim's default acceleration–deceleration functions. Second, the emissions model CMEM used in this study was developed using a relatively old vehicular fleet. Therefore, future research is needed to accommodate these limitations. In addition to that, there is a need to conduct additional research to address the following problems: First, future research should incorporate more comprehensive sustainability measures (e.g., safety and noise). Second, the variability of stop profiles' emissions used to compute the emissions-based stop penalty should be further researched using variance estimation techniques. Finally, future research should focus on developing a health risk index based on optimal signal timings to minimize specific emission type and compare it to optimal signal plans to mitigate other types of emissions to help achieve sustainability of human beings.

Author Contributions: Conceptualization, S.A., A.S. and N.D.; methodology, A.S. and S.A.; software, S.A. and N.D.; formal analysis, A.S., S.A. and N.D.; writing—original draft preparation, S.A., A.S. and N.D.; writing—review and editing, A.S., N.D. and S.A.; visualization, S.A., A.S. and N.D. All authors have read and agreed to the published version of the manuscript.

Funding: This research was partially funded by the Lake County (IL) Department of Transportation and the research contract on "Traffic Signal Optimization based on Fuel-consumption and Pollutant Emissions".

Data Availability Statement: Data and codes used for this research could be shared with the research community on request to the corresponding author.

Acknowledgments: The authors want to thank the U.S. Department of Energy's Vehicle Technologies Office and the Idaho National Laboratory for collecting and sharing the dataset used to develop the stochastic acceleration and deceleration functions used in this study. The authors also thank the Lake County DOT for their support.

Conflicts of Interest: The authors declare no conflict of interest.

References

1. EPA. Environmental Protection Agency. History of Air Pollution. Available online: https://www.epa.gov/air-research/history-air-pollution (accessed on 15 July 2021).
2. EPA. Environmental Protection Agency. How Does PM Affect Human Health? Available online: https://www3.epa.gov/region1/airquality/pm-human-health.html (accessed on 4 June 2021).
3. EPA. Environmental Protection Agency. Transportation Sector Emissions. Available online: https://www.epa.gov/ghgemissions/sources-greenhouse-gas-emissions#transportation (accessed on 4 June 2021).
4. EPA. Environmental Protection Agency. Smog, Soot, and Other Air Pollution from Transportation. Available online: https://www.epa.gov/transportation-air-pollution-and-climate-change/smog-soot-and-local-air-pollution (accessed on 4 June 2021).

5. EPA. Environmental Protection Agency. Carbon Pollution from Transportation. Available online: https://www.epa.gov/transportation-air-pollution-and-climate-change/carbon-pollution-transportation (accessed on 4 June 2021).
6. Stevanovic, A.; Stevanovic, J.; Zhang, K.; Batterman, S. Optimizing traffic control to reduce fuel consumption and vehicular emissions: Integrated approach with VISSIM, CMEM, and VISGAOST. *Transp. Res. Rec.* **2009**, *2128*, 105–113. [CrossRef]
7. "Brian" Park, B.; Yun, I.; Ahn, K. Stochastic optimization for sustainable traffic signal control. *Int. J. Sustain. Transp.* **2009**, *3*, 263–284. [CrossRef]
8. Rakha, H.; Ding, Y. Impact of stops on vehicle fuel consumption and emissions. *J. Transp. Eng.* **2003**, *129*, 23–32. [CrossRef]
9. Li, X.; Li, G.; Pang, S.S.; Yang, X.; Tian, J. Signal timing of intersections using integrated optimization of traffic quality, emissions and fuel consumption: A note. *Transp. Res. Part D Transp. Environ.* **2004**, *9*, 401–407. [CrossRef]
10. Zhao, H.; He, R.; Su, J. Multi-objective optimization of traffic signal timing using non-dominated sorting artificial bee colony algorithm for unsaturated intersections. *Arch. Transp.* **2018**, *46*, 85–96. [CrossRef]
11. Kwak, J.; Park, B.; Lee, J. Evaluating the impacts of urban corridor traffic signal optimization on vehicle emissions and fuel consumption. *Transp. Plan. Technol.* **2012**, *35*, 145–160. [CrossRef]
12. Liao, T.Y. A fuel-based signal optimization model. *Transp. Res. Part D Transp. Environ.* **2013**, *23*, 1–8. [CrossRef]
13. Courage, K.G.; Parapar, S.M. Delay and fuel consumption at traffic signals. *Traffic Eng.* **1975**, *45*, 23–27.
14. Ma, D.; Nakamura, H. Cycle length optimization at isolated signalized intersections from the viewpoint of emission. In *Traffic and Transportation Studies 2010*; American Society of Civil Engineers: Reston, VA, USA, 2010; pp. 275–284.
15. Akcelik, R. Fuel efficiency and other objectives in traffic system management. *Traffic Eng. Control* **1981**, *22*, 54–65.
16. Robertson, D.I. *TRANSYT: A Traffic Network Study Tool*; Road Resarch Laboratory: Berkshire, UK, 1969.
17. Albeck, J.; Husch, D. *Synchro Studio 7 Users Guide*; Trafficware: Sugar Land, TX, USA, 2006.
18. Robertson, D.I.; Lucas, C.F.; Baker, R.T. *Coordinating Traffic Signals to Reduce Fuel Consumption*; Transport Research Laboratory TRL Report LR934: Crowthorn, UK, 1980.
19. Stevanovic, A.; Shayeb, S.A.; Patra, S.S. Fuel Consumption Intersection Control Performance Index. *Transp. Res. Rec.* **2021**. [CrossRef]
20. Al Shayeb, S.; Stevanovic, A. Investigating Impacts of Various Operational Conditions on Fuel Consumption and Stop Penalty at Signalized Intersections. In Proceedings of the 100th Annual Meeting of the Transportation Research Board, Washington, DC, USA, 26 January 2021.
21. Banister, D. The sustainable mobility paradigm. *Transp. Policy* **2008**, *15*, 73–80. [CrossRef]
22. EPA. Environmental Protection Agency. Air Pollution Emissions Overview. Available online: https://www3.epa.gov/airquality/emissns.html (accessed on 4 June 2021).
23. Touratier-Muller, N.; Jaussaud, J. Development of Road Freight Transport Indicators Focused on Sustainability to Assist Shippers: An Analysis Conducted in France through the FRET 21 Programme. *Sustainability* **2021**, *13*, 9641. [CrossRef]
24. Karam, A.; Hegner Reinau, K. Evaluating the Effects of the A-Double Vehicle Combinations If Introduced to a Line-Haul Freight Transport Network. *Sustainability* **2021**, *13*, 8622. [CrossRef]
25. Hull Grasso, S.; Barnes, P.; Chavis, C. Bike Share Equity for Underrepresented Groups: Analyzing Barriers to System Usage in Baltimore, Maryland. *Sustainability* **2020**, *12*, 7600. [CrossRef]
26. Zhao, X.; Zhang, J.; Zhang, N.; Wong, Y.D.; Zhou, Y.; Meng, M. A GIS-CA Model for Planning Bikeways upon the Footpath Network. *Sustainability* **2021**, *13*, 8926. [CrossRef]
27. Croce, A.I.; Musolino, G.; Rindone, C.; Vitetta, A. Estimation of Travel Demand Models with Limited Information: Floating Car Data for Parameters' Calibration. *Sustainability* **2021**, *13*, 8838. [CrossRef]
28. Přibyl, P.; Janota, A.; Spalek, J.; Faltus, V. Knowledge System Supporting ITS Deployment. *Sustainability* **2021**, *13*, 6407. [CrossRef]
29. Gamboa-Rosales, N.K.; Celaya-Padilla, J.M.; Hernandez-Gutierrez, A.L.; Moreno-Baez, A.; Galván-Tejada, C.E.; Galván-Tejada, J.I.; González-Fernández, E.; Gamboa-Rosales, H.; López-Robles, J.R. Visualizing the Intellectual Structure and Evolution of Intelligent Transportation Systems: A Systematic Analysis of Research Themes and Trends. *Sustainability* **2020**, *12*, 8759. [CrossRef]
30. Claffey, P.J. *Passenger Car Fuel Conservation*; National Technical Information Service: Springfield, VA, USA, 1976.
31. Smith, K.; Wood, K.; Ash, A. Managing emissions from vehicles in urban systems. In Proceedings of the AET European Transportation Conference, Homerton College, Cambridge, UK, 10–12 September 2001.
32. Rubin, J.I.; Kean, A.J.; Harley, R.A.; Millet, D.B.; Goldstein, A.H. Temperature dependence of volatile organic compound evaporative emissions from motor vehicles. *J. Geophys. Res. Atmos.* **2006**, *111*, D03305. [CrossRef]
33. Zhang, Q.; Wu, L.; Fang, X.; Liu, M.; Zhang, J.; Shao, M.; Lu, S.; Mao, H. Emission factors of volatile organic compounds (VOCs) based on the detailed vehicle classification in a tunnel study. *Sci. Total. Environ.* **2018**, *624*, 878–886. [CrossRef]
34. Frey, H.C.; Unal, A.; Rouphail, N.M.; Colyar, J.D. On-road measurement of vehicle tailpipe emissions using a portable instrument. *J. Air Waste Manag. Assoc.* **2003**, *53*, 992–1002. [CrossRef]
35. EPA. Environmental Protection Agency. Basic Information about Carbon Monoxide (CO) Outdoor Air Pollution. Available online: https://www.epa.gov/co-pollution/basic-information-about-carbon-monoxide-co-outdoor-air-pollution#Effects (accessed on 4 June 2021).
36. EPA. Environmental Protection Agency. Overview of Greenhouse Gases. Available online: https://www.epa.gov/ghgemissions/overview-greenhouse-gases#carbon-dioxide (accessed on 4 June 2021).

37. EPA. Environmental Protection Agency. Effects of Acid Rain. Available online: https://www.epa.gov/acidrain/effects-acid-rain (accessed on 4 June 2021).
38. Portmann, R.W.; Daniel, J.S.; Ravishankara, A.R. Stratospheric ozone depletion due to nitrous oxide: Influences of other gases. *Philos. Trans. R. Soc. B Biol. Sci.* **2012**, *367*, 1256–1264. [CrossRef]
39. EPA. Environmental Protection Agency. Basic Information about NO2. Available online: https://www.epa.gov/no2-pollution/basic-information-about-no2#Effects (accessed on 4 June 2021).
40. EPA. Environmental Protection Agency. Ground-Level Ozone Basics. Available online: https://www.epa.gov/ground-level-ozone-pollution/ground-level-ozone-basics (accessed on 4 June 2021).
41. Panis, L.I.; Broekx, S.; Liu, R. Modelling instantaneous traffic emission and the influence of traffic speed limits. *Sci. Total Environ.* **2006**, *371*, 270–285. [CrossRef] [PubMed]
42. Rakha, H.; Ahn, K.; Trani, A. Development of VT-Micro model for estimating hot stabilized light duty vehicle and truck emissions. *Transp. Res. Part D Transp. Environ.* **2004**, *9*, 49–74. [CrossRef]
43. Roess, R.P.; Prassas, E.S.; McShane, W.R. *Traffic Engineering*; Pearson/Prentice Hall: Hoboken, NJ, USA, 2004.
44. Oda, T.; Kuwahara, M.; Niikura, S. Traffic Signal Control for Reducing Vehicle Carbon Dioxide Emissions on an Urban Road Network. In Proceedings of the 11th World Congress on ITS, Nagoya, Japan, 1–8 October 2004.
45. Zhang, L.; Yin, Y.; Chen, S. Robust signal timing optimization with environmental concerns. *Transp. Res. Part C Emerg. Technol.* **2013**, *29*, 55–71. [CrossRef]
46. Lv, J.; Zhang, Y.; Zietsman, J. Investigating emission reduction benefit from intersection signal optimization. *J. Intell. Transp. Syst.* **2013**, *17*, 200–209. [CrossRef]
47. Khalighi, F.; Christofa, E. Emission-based signal timing optimization for isolated intersections. *Transp. Res. Rec.* **2015**, *2487*, 1–4. [CrossRef]
48. Osorio, C.; Nanduri, K. Urban transportation emissions mitigation: Coupling high-resolution vehicular emissions and traffic models for traffic signal optimization. *Transp. Res. Part B Methodol.* **2015**, *81*, 520–538. [CrossRef]
49. Han, K.; Liu, H.; Gayah, V.V.; Friesz, T.L.; Yao, T. A robust optimization approach for dynamic traffic signal control with emission considerations. *Transp. Res. Part C Emerg. Technol.* **2016**, *70*, 3–26. [CrossRef]
50. Lighthill, M.J.; Whitham, G.B. On kinematic waves II. A theory of traffic flow on long crowded roads. Proceedings of the Royal Society of London. Series, A. *Math. Phys. Sci.* **1955**, *229*, 317–345.
51. Richards, P.I. Shock waves on the highway. *Oper. Res.* **1956**, *4*, 42–51. [CrossRef]
52. PTV Vissim 10 User Manual, PTV Group. Available online: https://usermanual.wiki/Document/Vissim20102020Manual.1098038624.pdf (accessed on 22 February 2018).
53. Frey, H.C.; Rouphail, N.M.; Unal, A.; Colyar, J.D. *Emissions Reduction through Better Traffic Management: An Empirical Evaluation Based upon on-Road Measurements*; FHWA/NC/2002-001, Final Report; North Carolina State University: Raleigh, NC, USA, 2001.
54. Scora, G.; Barth, M. *Comprehensive Modal Emission Model (cmem) Version 3.01 User's Guide*; University of California: Riverside, CA, USA, 2006.
55. Fisher, R.A. The arrangement of field experiments. In *Breakthroughs in Statistics*; Springer: New York, NY, USA, 1992; pp. 82–91.
56. Barth, M.; An, F.; Younglove, T.; Scora, G.; Levine, C.; Ross, M.; Wenzel, T. The development of a comprehensive modal emissions model. *NCHRP Web-Only Doc.* **2000**, *122*. Available online: https://trid.trb.org/view/859153 (accessed on 1 September 2021).
57. Hancock, M.W.; Wright, B. *A Policy on Geometric Design of Highways and Streets*; American Association of State Highway and Transportation Officials: Washington, DC, USA, 2013.
58. An, F.; Barth, M.; Norbeck, J.; Ross, M. Development of comprehensive modal emissions model: Operating under hot-stabilized conditions. *Transp. Res. Rec.* **1997**, *1587*, 52–62. [CrossRef]
59. Rakha, H.; Ahn, K.; Trani, A. Comparison of MOBILE5a, MOBILE6, VT-MICRO, and CMEM models for estimating hot-stabilized light-duty gasoline vehicle emissions. *Can. J. Civ. Eng.* **2003**, *30*, 1010–1021. [CrossRef]
60. Barth, M.; Malcolm, C.; Younglove, T.; Hill, N. Recent validation efforts for a comprehensive modal emissions model. *Transp. Res. Rec.* **2001**, *1750*, 13–23. [CrossRef]
61. Stevanovic, A.; Gundogan, F. Calibration of micro-simulation models for ITS applications. In Proceedings of the 19th ITS World Congress, Vienna, Austria, 22–26 October 2012.
62. Partners, Crash Avoidance Measures. Traffic Optimization for Signalized Corridors (TOSCo) Phase 1 Project Report. 2019. Available online: https://pronto-core-cdn.prontomarketing.com/2/wp-content/uploads/sites/2896/2020/02/TOSCo_Phase_1_Final_Report_-_CAMP_WEBSITE.pdf (accessed on 1 September 2021).
63. Sakoe, H.; Chiba, S. Dynamic programming algorithm optimization for spoken word recognition. *IEEE Trans. Acoust. Speech Signal Process.* **1978**, *26*, 43–49. [CrossRef]
64. Hartigan, J.A.; Wong, M.A. Algorithm AS 136: A k-means clustering algorithm. *J. R. Stat. Soc. Ser. C (Appl. Stat.)* **1979**, *28*, 100–108. [CrossRef]
65. INL. Idaho National Laboratory. 2021. Available online: https://inl.gov/ (accessed on 1 September 2021).
66. Department of Energy. Available online: https://www.energy.gov/ (accessed on 1 September 2021).
67. McConville, G.P.; Cook, H.E. Examining the Trade-Off between Automobile Acceleration Performance and Fuel Economy. *SAE Trans.* **1996**, *105*, 37–45.
68. Thorndike, R.L. Who belongs in the family? *Psychometrika* **1953**, *18*, 267–276. [CrossRef]

69. Tan, W.; Li, Z.C.; Tan, Z.J. Modeling the effects of speed limit, acceleration, and deceleration on overall delay and traffic emission at a signalized intersection. *J. Transp. Eng. Part A Syst.* **2017**, *143*, 04017063. [CrossRef]
70. Ding, S.; Chen, X.; Yu, L.; Wang, X. Arterial Offset Optimization Considering the Delay and Emission of Platoon: A Case Study in Beijing. *Sustainability* **2019**, *11*, 3882. [CrossRef]
71. Alonso, B.; Pòrtilla, Á.I.; Musolino, G.; Rindone, C.; Vitetta, A. Network Fundamental Diagram (NFD) and traffic signal control: First empirical evidences from the city of Santander. *Transp. Res. Procedia* **2017**, *27*, 27–34. [CrossRef]
72. Alonso, B.; Ibeas, Á.; Musolino, G.; Rindone, C.; Vitetta, A. Effects of traffic control regulation on Network Macroscopic Fundamental Diagram: A statistical analysis of real data. *Transp. Res. Part A Policy Pract.* **2019**, *126*, 136–151. [CrossRef]